Philipp Schmid, BSc

Material Properties of Aryl Decorated Tin Nanoparticles from Different Synthetic Pathways

Master's Thesis

to achieve the university degree of

Diplom-Ingenieur

Master's degree programme: Technical Chemistry

submitted to

Graz University of Technology

Supervisors
Univ.-Prof. Dipl.-Chem. Dr.rer.nat. Frank Uhlig
Ph.D. Ana Torvisco Gómez

Institute of Inorganic Chemistry

Graz, 24.09.2020

Abstract

Over the course of this work, aryl@Sn nanoparticles were synthesized through dehydrogenative coupling of arylSnH_3. The reactions were carried out in the different solvents toluene, DME, benzene and cyclohexane which vary in polarity, donicity and boiling point. Energy for the reaction was provided in different ways: through mechanical stirring at ambient temperature, conventional heating, microwave radiation and ultra sonication. The materials were synthesized both with and without the aid of the amine base catalyst TMEDA.

Analysis of all samples using SAXS showed that the correlation length, which might correspond to the size of the nanoparticle or of its metallic core, depends both on the donicity of the solvent and the presence of a TMEDA catalyst, with faster reactions in a donating solvent and/or with a catalyst decreasing the correlation length. WAXS measurements of the same materials showed characteristic Sn(0) scattering for samples synthesized without a catalyst, indicating more Sn(0) in the nanoparticle core and a higher metallic character. Some samples synthesized in cyclohexane showed an intermediate behavior between nanoparticles with high and low metallic character.

Elemental analysis showed the loss of organic residues during nanoparticle formation, resulting in nanoparticles containing more tin than aryl. A significant difference between particles with high and low metallic character was also found, with the latter containing higher remaining amounts of the aryl. The choice of solvent also plays a role in the ultimate composition, with more donating solvents causing a higher retention of organic substituents. Despite the clear presence of general trends, variance of elemental composition between samples is high and probably also depends on less clearly defined factors than just solvent, catalyst and temperature.

Scanning electron microscopy largely confirmed previous findings, showing that a faster synthetic process with a catalyst leads to more regular, larger, spherical structures, whereas a slower synthetic process leads to irregular agglomerations. Samples with an intermediate behavior were found to contain a mixture of the two morphologies.

Kurzfassung

Im Verlauf dieser Arbeit wurden aryl@Sn Nanopartikel durch dehydrierende Kopplung von arylSnH_3 hergestellt. Diese Reaktionen wurden in den verschiedenen Lösungsmitteln Toluol, DME, Benzen und Cyclohexan durchgeführt, welche sich hinsichtlich ihrer Polarität, Donizität und ihrer Siedepunkte unterscheiden. Die Reaktionsenergie wurde auf verschiedene Arten zur Verfügung gestellt: Durch Umgebungswärme, konventionelles Erhitzen, Mikrowellenstrahlung und Ultraschall. Die Materialien wurden sowohl mit als auch ohne die Hilfe des Aminbasenkatalysators TMEDA synthetisiert.

Die Analyse aller Proben mittels SAXS zeigte, dass die Korrelationslänge, welche die Größe der Nanopartikel oder deren metallischen Kerns sein könnte, sowohl von der Donizität des Lösungsmittels als auch der Anwesenheit des TMEDA-Katalysators abhängt, wobei schnellere Reaktionen in donierenden Lösungsmitteln und/oder mit Katalysator eine kleinere Korrelationslänge zur Folge haben. Die Korrelationslänge von Proben die ohne TMEDA hergestellt wurden konnte nicht genau bestimmt werden, da sich das Signal mit der Streuung größerer Partikel überlagerte. WAXS Messungen der gleichen Materialien zeigten charakteristische Sn(0) Streuungen in Proben die ohne Katalysator hergestellt wurden, was auf einen höheren Gehalt an Sn(0) im Kern und einen stärkeren metallischen Charakter hinweist. Manche Proben die in Cyclohexan synthetisiert wurden zeigten ein Verhalten zwischen dem von Nanopartikeln mit starkem und solchen mit schwachem metallischen Charakter.

Die Elementaranalyse zeigte einen Verlust von organischen Resten im Zuge der Bildung der Nanopartikel, was zu Nanopartikeln die mehr Zinn als Aryl enthielten führte. Ein signifikanter Unterschied zwischen Partikeln mit starkem und schwachem metallischen Charakter wurde ebenfalls gefunden, wobei letztere mehr organisches Material beinhalten. Die Wahl des Lösungsmittels spielt in der finalen Zusammensetzung ebenso eine Rolle, wobei polarere, stärker donierende Lösungsmittel zu einer größeren Menge an verbleibenden organischen Subsituenten führen. Diese generellen Trends sind zwar gut zu beobachten, die Varianz bei der Zusammensetzung verschiedener Proben ist aber hoch und hängt vermutlich auch von weniger klar definierten Faktoren als nur Lösungsmittel, Katalysator und Temperatur ab.

Rasterelektronenmikroskopie bestätigte größtenteils frühere Erkenntnisse, wonach

schnellere synthetische Prozesse mit einem Katalysator zu regulärere, größeren, kugelförmigen Strukturen führen, wohingegen langsamere Syntheseprozesse eine irreguläre Aggolmeration zur Folge haben. Proben mit charakteristiken zwischen einem starken und einem schwachen metallischen Charakter bestehen aus einer Mischung der beiden morphologischen Strukturen.

EIDESSTATTLICHE ERKLÄRUNG

Ich erkläre an Eides statt, dass ich die vorliegende Arbeit selbstständig verfasst, andere als die angegebenen Quellen/Hilfsmittel nicht benutzt, und die den benutzten Quellen wörtlich und inhaltlich entnommenen Stellen als solche kenntlich gemacht habe. Das in TUGRAZonline hochgeladene Textdokument ist mit der vorliegenden Masterarbeit identisch.

AFFIDAVIT

I declare that I have authored this thesis independently, that I have not used other than the declared sources/resources, and that I have explicitly indicated all material which has been quoted either literally or by content from the sources used. The text document uploaded to TUGRAZonline is identical to the present master‘s thesis.

Datum/Date	Unterschrift/Signature

Danksagung

Zu Beginn dieses Abschnittes möchte ich mich bei meinem Betreuer Frank Uhlig für die Aufnahme in seine Arbeitsgruppe und die Möglichkeit hier meine Masterarbeit zu verfassen bedanken. Danke auch für die Ratschläge wenn ich irgendwo anstand sowie für die Zeit die du dir immer wieder für hilfreiche Gespräche nimmst, sei es über die Arbeit selbst, Tricks und Arbeitstechniken, Anstellungsverhältnisse oder einfach Organisatorisches.

Further thanks goes to my second supervisor, Ana Torvisco. You always had an open ear for me when any problems came along, be it during the lab work or during the actual writing of the thesis. You helped me out of dead ends, showed me where to keep trying and guided me to successful completion of this thesis. When I had any special requests you pointed me to the right people. Thanks also for the food and sweets you provided me with, sugar is what keeps me going.

Großer Dank gilt auch meiner Vorgängering Susanne Reischauer: Du hast mir nicht nur schon lange vor Beginn der Masterarbeit mit Unterlagen, Ausarbeitungen und Altfragen durchs Studium geholfen, du hast mich auch überhaupt erst zur AG Uhlig gebracht und mit deiner Masterarbeit die Grundlage für meine gelegt. Danke auch an Michael Traxler für die Zeit die du nach Susis Weggang geopfert hast um mir bei der Einarbeitung zu helfen.

Vielen Dank an Manfred, nicht nur für die Durchführung der SAXS und WAXS Messungen sondern auch für Hilfe bei der Auswertung der Daten und Erklärungen zum besseren Verständnis der Methode, an Moni für die Elementaranalysen, Chemikalien und den Laborbedarf sowie an Babsi und Marit, die der gesamten Arbeitsgruppe im Hintergrund viele Steine aus dem Weg räumen.

Danke an alle Kolleginnen und Kollegen die mich unterstützt und mir Ratschläge gegeben haben, an Beate, Gernot und Stefan für ihr Mentoring aber ganz besonders an diejenigen die über die Arbeit hinaus auch zu Freunden wurden und somit für emotionale Unterstützung in schwierigen Phasen und zahlreiche außeruniversitäre Aktivitäten

zur Entspannung verantwortlich sind: Benjamin, Doris, Christoph, Feri, Philipp und Yaiza.

Viel verdanke ich natürlich auch allen meinen Freunden und Freundinnen, die mir seit teilweise über einem Jahrzehnt zur Seite stehen, ihr wisst was und wie viel ihr alles für mich gemacht habt: Anja, Babsi & Babsi, Daniel, David, Dominik, Hamster, Hannah, Luzi, Manni, Mottl, Niko, Philipp, Sandra, Tamara und Werner.

Zu guter letzt möchte ich mich ganz besonders bei meinen Eltern bedanken, die mich immer schon ermutigt haben mein Bestes zu geben und mir das Studium mit finanzieller und emotionaler Unterstützung durch alle Dummheiten hindurch überhaupt erst ermöglicht haben.

Contents

1 Introduction

As the role electricity and electronic devices play in daily live continues to increase, so does the need for more efficient power storage devices. For hand held devices and electric vehicles, the Li-ion battery has been established as the primary choice. However, the typically used graphite intercalation electrode severely limits the achievable capacity, with a theoretic maximum of 372 mA*h/g [1]. Tin offers a much higher value of 944 mA*h/g [2] but suffers from low cycle stability due to great volume changes [3]. One line of research to alleviate this problem is the use of tin nanoparticles, encapsulated by a matrix capable of buffering the expansion and contraction of the material. It was previously discovered[4] that aryltin trihydride undergoes rapid dehydrogenative coupling in the presence of an amine catalyst such as TMEDA, forming aryl decorated tin nanoparticles with a core of "naked" tin atoms in the oxidation state zero, connected only to other tin atoms. The aromatic groups could further improve the electronic properties through $\sigma - \pi$ delocalization and narrowing of the band gap. Unfortunately, these nanoparticles did not show significant conductivity. Further investigations[5] discovered signals corresponding to white tin during WAXS analysis of materials synthesized under certain reaction conditions where no amine catalyst was used, resulting in an increased reaction time in the order of days to weeks. This suggests the presence of a greater amount of Sn(0), enough to cause the characteristic scattering pattern, in the core of the nanoparticles, increasing their metallic character. It therefore became the objective of this work to further elaborate on the cause of WAXS signals appearing, confirm their identity as white tin and optimize the reaction conditions for increased metallic character of the nanoparticles. Further interest lay in investigation of the resulting materials using elemental analysis and SEM to gain further information about their structure and link possible differences to their composition. The final goal of the thesis was to investigate the electronic properties of the tin polymers and identify suitable candidates for investigation in a battery. Figure 1.1 shows the different parameters of the coupling reaction which were changed to generate a variety of materials.

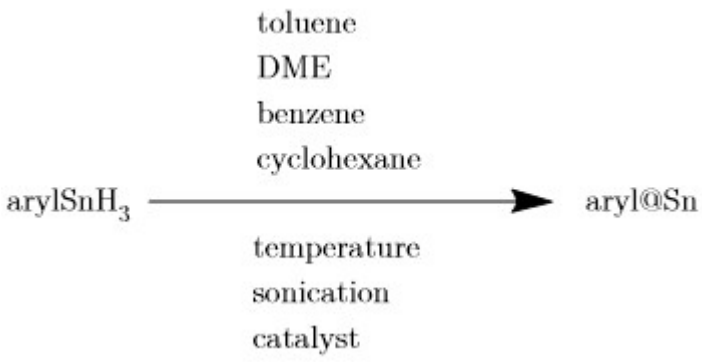

Figure 1.1: Different reaction conditions in the deghydrogenative coupling reactions of aryltin trihydrides

2 Theoretical Background

2.1 Organotin Hydrides

2.1.1 History of Organotin Hydrides

Organotin hydrides are a form of organic tin compounds and have the general structure R_nSnH_{4-n}. The first and most basic member of the family, stannane (SnH_4), was synthesized in 1920 by Paneth [6], by treating a Sn-Mg alloy with acids. They also obtained the same compound through the use of cathodic reduction [7], but high complexity and low yield made both methods inefficient. Due do its lack of organic substituents, it is not technically considered to be an organotin compound. The first true organotin compound, Me_3SnH, was synthesized in 1922 by Kraus and Greer [8], using the method depicted in Figure 2.1. Chambers and Scherer were the first to characterize an aromatic tin hydride (Ph_3SnH) using the same method [9]. Despite its inconvenience, it remained the only functional strategy for synthesis of organotin hydrides util 1947, severely limiting research into the compound class.

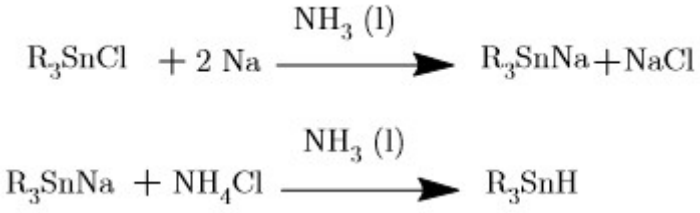

Figure 2.1: The synthesis of organotin hydrides as developed by Kraus and Greer

More recently, Finholt *et al.* developed a new, more convenient route using LAH ($LiAlH_4$, which is shown in Figure 2.2 [10]. Using this method, they were the first to synthesize organotin di- and monohydrides. The comparably low time and effort required for this process led to a host of new organotin hydrides being succesfully synthesized over the next years [11–14], and as of today it remains the prevalent synthetic strategy [15].

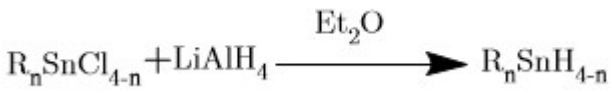

Figure 2.2: The synthesis of organotin hydrides as developed by Finholt *et al.*

2.1.2 Properties of Organotin Hydrides

The tin hydrogen bond has a low dissociation energy, making it labile to both temperature and the influence of oxygen, often decomposing even at room temperature under an inert atmosphere and decaying rapidly to a white powder, possibly SnO_2 upon contact with air [12]. The stability of these compounds increase the more organic substituents are substituted for hydrogen atoms [8, 10, 12], with SnH_4 consequentially being the most instable compound of the family and igniting upon contact with air. The compounds can be further stabilized through increasing the steric demand of the organic ligands, with bulky aromatic ligands offering the highest stabilization and enabling characterization of the resulting solids using single crystal X-ray diffraction [16, 17]. Organotin hydrides act as strong reducing agents, being able to reduce a variety of different functional groups such as organic halides, amines and ketones [18, 19]. Organotin hydrides are also able to undergo hydrostannylation with organic compounds containing multiple bonds, thus expanding the library of available organotin compounds [20].

2.2 Polymerization of Organotin Compounds

Although oligomers can be formed by many different metals, so far tin is the only material successfully used for the synthesis of polymers with a main chain consisting exclusively of metal atoms [21]. The resulting macromolecules are called polystannanes and both 2D and 3D variations are known. A variety of different synthetic strategies towards these materials have been developed.

2.2.1 Wurtz Reaction

The first successful synthesis of a polystannane was performed in 1852 by Löwig [22], who reacted Iodoethane with an Na/Sn alloy under different conditions. However, he only described one resulting compound, Et_2Sn [23], with Strecker later correctly labeling other compounds in the mixture as oligomeric and polymeric stannanes $[Et_2Sn]_n$ [24]. The same procedure was later repeated by Cahours [25]. This constitutes a Wurtz reaction which uses halogenides and elemental sodium to couple two partners in a halogen-metal

exchange as seen in Figure 2.3, although it can also be performed with metals other than sodium [26].

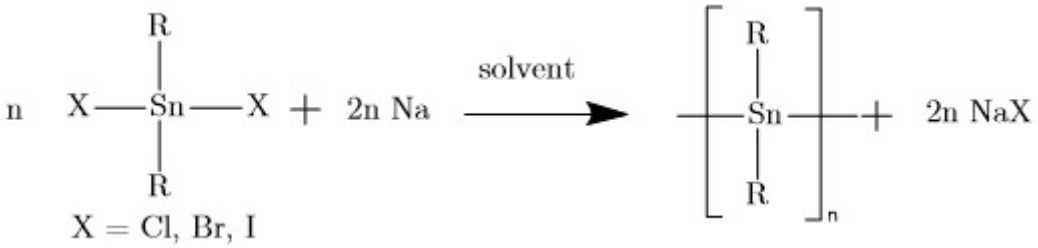

Figure 2.3: General Wurtz coupling of organotins

The Wurtz reaction remains in use as a way toward oligo- and polystannanes to the present day, with toluene and NH_3(l) used as solvents [27–32]. It is able to generate polymers with high molar masses of M_n up to 10^6 [29]. The main drawback lies in the low yield, high polydispersity, low functional group tolerance, as well as the formation of cyclic oligomers as a byproduct [21, 33, 34].

2.2.2 Condensation

In 1964, Neumann and Schneider pioneered the generation of organic di-, tri- and polystannanes through a condensation reaction by combining tin hydrides with tin oxides [41]. They later expanded this method to tin amides as educt [42], albeit only generating oligostannanes in the process. Uhlig and coworkers also used condensation with amines to form cyclic silane-stannane co oligomers [43]. Foucher and colleagues synthesized and characterized alternating linear tin co-oligomers [44] and co-polymers [45, 46] by combining tin dihydrides and tin diamides in stoichiometric amounts, being the first to succesfully create a polymer *via* condensation of amides. Figure 2.4 shows their approach. While it led to lower molecular weights, it also caused lower polydispersity. Their use of aromatic and aliphatic residues improved stability respectively solubility compared to the homopolymers.

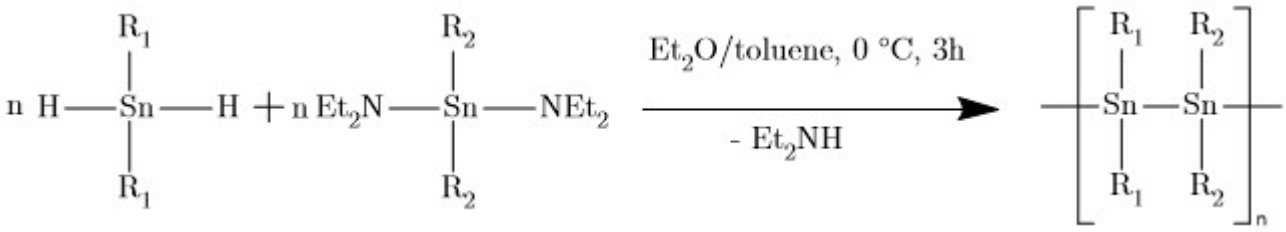

Figure 2.4: Polycondensation of tinhydrides and amides employed by Foucher *et al.*

2.2.3 Organometal Catalyzed Dehydrogenation

The many drawbacks of Wurtz type reactions severely limited its applicability for research purposes. Therefore, inspired by similar silicone and germanium chemistry, the working group of Tilley developed a polymerization method for dibutyltin dihydrides using an organometallic zirconium catalyst [27, 47–49].

Many others followed this approach due to its convenience, generating numerous di-, cyclo-, oligo- and polystannanes through use of a variety of catalysts, such as transition metals based on zirconium, hafnium, molybdenum, iron, platinum and rhodium (Wilkinson's Catalyst) [32, 50–55], as well as lanthanides [17]. Figure 2.5 depicts the basic reaction scheme. Through optimization of the catalyst, the reaction could be influenced to generate no cyclic oligomer impurities whatsoever [56].

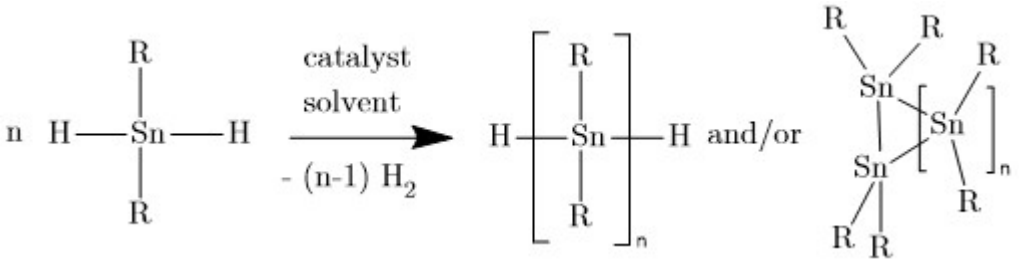

Figure 2.5: Dehydrogenative coupling of organotin hydrides using an organometallic catalyst

2.2.4 Electrolytic Reaction

The second method using tin halogenides as educt for polymerization is electrochemical synthesis. The general reaction formula is depicted in Figure 2.6. It was pioneered by Okano *et al.* in 1998 who used it to produce poly(dibutylstannane) and

poly(dioctylstannane) [57]. In a different work, Okano *et al.* also became the first group to successfully create 3D polystannane networks from tin trichlorides with organic substituents Me, Bu, Oct, and Ph [58]. The products suffered from impurities caused by unreacted tin-halide bonds that are difficult to get rid of and other working groups have only used it for electroplating in electrochemical studies [34].

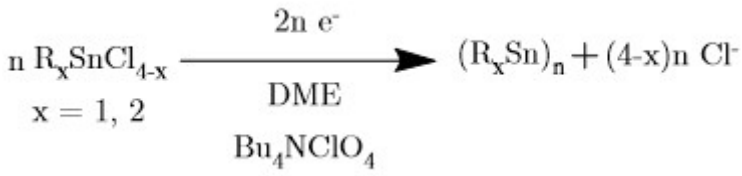

Figure 2.6: General electrolytic coupling of organotins

2.2.5 Thermal Dehydrogenation

After initial reports showed the possibility to produce $Bu_3SnSnBu_3$ without solvent or catalyst by simply heating it [59], this approach was expanded to include the synthesis of polystannanes [60]. Due to the weak nature of the Sn-H bond, thermal dehydrogenation proceeds even in solution at room temperature, although the required reaction time is high [61]. The thermal dehydrocoupling approach is viable for both organotin dihydrides [59–61] and trihydrides [5] (Figure 2.7).

Figure 2.7: General approach for the thermal dehydrogenation of organotin hydrides

2.2.6 Amine Base Catalyzed Dehydrogenation

Neumann and König first discovered the possibility to use dimethylformamide and pyridine as catalysts for the dehydrogenative coupling of tin hydrides towards cyclic oligomers, with Ph_2SnH_2 as their monomer [35, 36]. Davis and Ossei-Kissi elaborated this mechanisms with the formation of a distannane as their model reaction, citing a radical chain mechanism [37]. In 2011, Uhlig and Coworkers used TMEDA for the first time in a comparison of different catalysts for tin coupling. They found it to be bad at

polymerizing pure alkyltin dihydrides but efficient for the dehydrogenation of dihydrides with aromatic or mixed substituents[32].

Sindlinger and his coworkers tried coupling an organotin trihydride using amine bases. They used aromatic substituents with a high steric demand such as triisopropylphenyl and bis(triisopropylphenyl)phenyl. The steric demand stabilized the molecules and prevented the reaction from proceeding to polymerization, yielding distannanes RH_2SnSnH_2R, RSnH both as a base adduct and uncoordinated, depending on the used base and it's concentration. Upon stoichiometric reaction, they were able to create a tin cluster of the composition R_6Sn_6 [38, 39]. They later proceeded to synthesize more tin clusters by varying the substituent and the reaction conditions [40].

With less sterically demanding substituents, a variety of amine bases lead to polymerization to aryl decorated tin nanoparticles. Notably, not only hydrogen but also some R groups are abstracted in this process, resulting in a core of elemental Sn(0) (Figure 2.8), as shown by Zeppek from the Uhlig working group in her doctoral thesis [4]. When used for catalytic dehydrogenation, amine bases coordinate to the tin atom, weakening and elongating the Sn-H bond in the process. This significantly increases thermal cleavage of the bond, H_2 formation and subsequent polymerization.

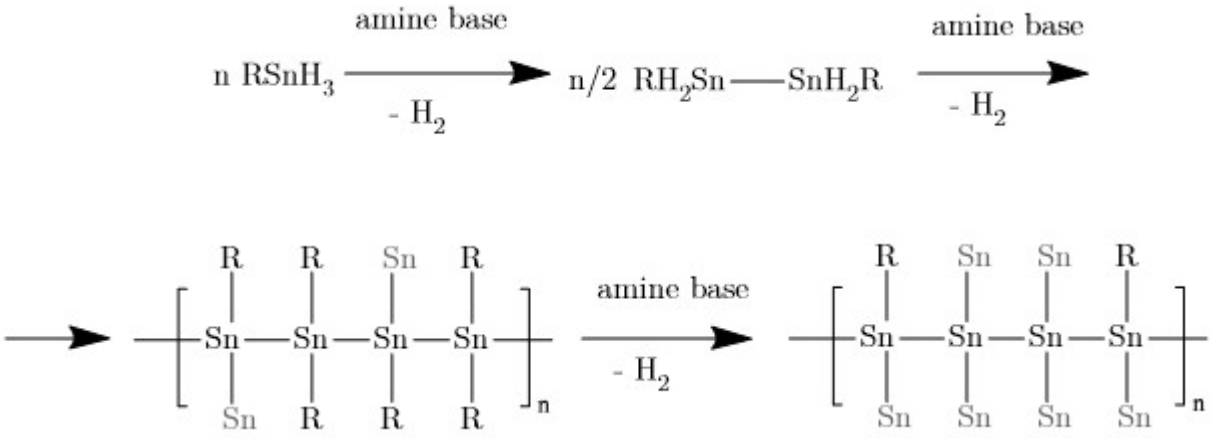

Figure 2.8: Polymerization of organotin trihydrides to yield nanoparticles with a metallic core

2.3 2D Tin Nanowires

Due to the (distorted) tetrahedral bond angles at the tetravalent tin atom, linear polystannanes do not exist in a straight line. Instead, they may arrange themselves

either in a planar zig-zag shape (all *trans*) or as a helix (*gauche*) [21]. The tin atoms are covalently bonded to each other, resulting in σ conjugation along the metallic backbone and the creation of a delocalized valence band due to the overlap of $5p_x$ orbitals. A delocalized conduction band comprised of $5p_y$ and 5s orbitals similarly exists [47, 62]. The materials can thus be regarded as tin nanowires with an organic jacket or "molecular metal wires" [63]. A few examples of this type of material are displayed in Figure 2.9.

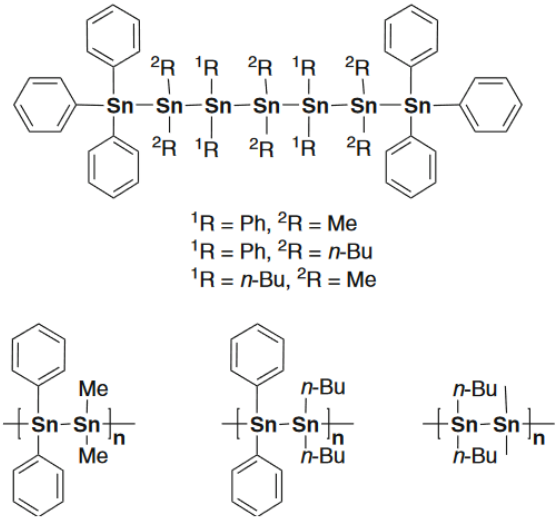

Figure 2.9: Structure of various 2D-Tin oligomers and nanowires [44]

The band gap decreases with chain length through increasing delocalization [29] and chain conformation, because the all *trans* alignment provides better orbital overlap [48, 62]. A third important characteristic is the main chain bond angle. Wider bond angles once again provide more favorable overlap of orbitals and a lower energy gap. It can be achieved through bulky substituents or application of pressure [44, 48]. Aromatic substituents cause a further lowering of the band gap through additional $\sigma - \pi$ conjugation [48, 49]. Although overlapping bands have been predicted to be the case for main chain bond angles over 150°, this is not usually the case [44]. The conductivity of tin nanowires increases with temperature [54] and can be improved through doping [27], which is in line with the behavior of semiconductors. Aliphatic 2D tin nanowires are soluble in common organic solvents such as benzene, toluene and THF [27, 54, 56, 64]. Aromatic polystannanes such as $[Ph_2Sn]_n$ on the other hand are insoluble [17, 30–32]. Their solubility can however be improved through either substitutions at the aromatic ring [32, 49] or copolymerization with aliphatic tinhydrides [30, 45]. A lack of solubility creates

challenges during both processing and characterization of final materials [21]. In order to identify (soluble) polystannanes, NMR spectroscopy can be employed. They differentiate themselves from cyclic oligomers through lower chemical shifts during ^{119}Sn-spectroscopy [27, 56], although shifts are stronlgy dependent on the R group [21]. Due to their low band gap, polystannanes display a characteristic absorption maximum in the UV-vis range, resulting in a yellow to orange color. λ_{max} depends of course on the size of the band gap, and commonly lies in the range of 370-400 nm for aliphatic subsituents and 420-470 nm for aromates [27, 32, 34, 54], although more extreme values are possible with strong donating or withdrawing groups [28, 49]. Sn-Sn bonds have lower energy than the group 14 elements with lower atomic number [44], resulting in a lack of stability. Linear polystannanes are both air and light sensitive [49], although their stability can be improved through aromatic substituents [32].

2.4 3D Tin Nanoparticles

Ligand stabilized clusters of group 14 elements following the general formula Sn_nR_n have been known for a while [65]. In 1989, Sita and Bickerstaff reported a ligand stabilized cluster containing "naked" tin atoms (meaning unbonded to atoms other than tin) through thermolysis of cyclotristannane [66]. Other groups followed, succesfully synthesizing clusters with fewer ligands than metal atoms of the formula Sn_nR_n with n>m, employing methods such as thermolysis or reduction of the metal halide or amide with alkaline metals [67–69]. In these compounds, the naked metal atoms provide additional free electrons, facilitating delocalization and band gap reduction [70]. As opposed to these structurally well defined, molecular tin nanoparticles, Zeppek was the first to report in 2015 the dehydrogenative coupling of aryltin trihydrides using amine bases as catalysts, yielding aryl decorated tin nanoparticles [4]. During this reaction, the originally colorless educt starts turning yellow and orange. As with linear tin polymers (see above), this indicates an increasing delocalization of electrons over the different tin atoms, narrowing the band gap and causing a bathochromic shift into the visible wavelength spectrum. However, in contrast to the linear case, the color change does not stop there, continuing instead to brown and black, implying broad absorption over the entire visible spectrum (Figure 2.10).

The resulting solid material was found to be insoluble in any common solvent, preventing NMR, GPC or GC/MS analysis. GC/MS and NMR analysis of the filtrate showed presence of the free aromatic substituent R, showing that it had, to some degree, been cleaved off during the reaction. This was further underlined by elemental analysis of the material, which returned lower percentages of C and H than would be expected for pure $[RSn]_n$

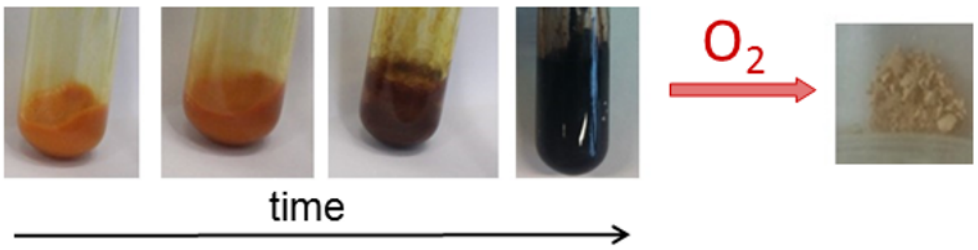

Figure 2.10: Color change upon reaction of $RSnH_3$ with TMEDA at room temperature [71]

[4]. Loss of the aryl residue also serves to explain the black color, which is caused by the Sn(0) scaffold in the core of the nanoparticles (see Chapter 1). SEM analysis showed the material to be made from spheres with a diameter in the low micrometer range (Figure 2.11) while FESEM revealed these spheres to me made from yet smaller spheres with a diameter of 7-30 nm (Figure 2.12). This was also confirmed by TEM measurements [4].

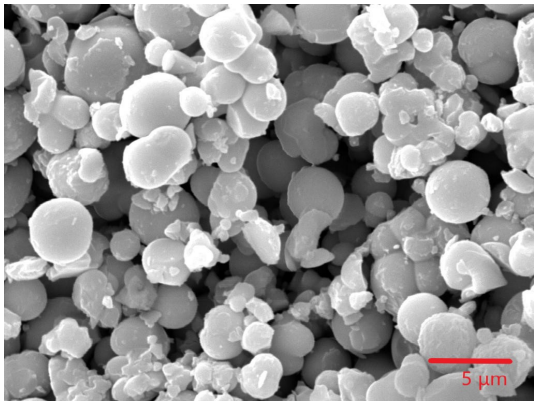

Figure 2.11: Morphology of *o*-tolyl@Sn under SEM [5]

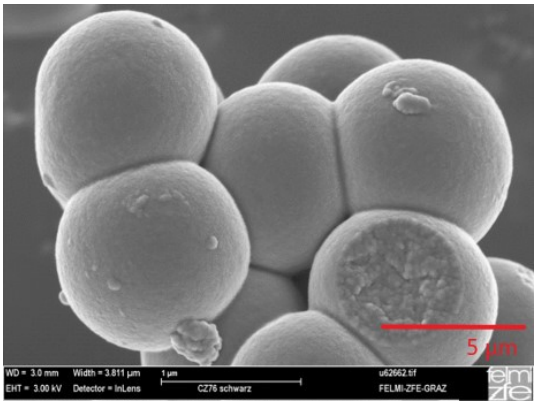

Figure 2.12: Morphology of *o*-tolyl@Sn under FESEM [4]

In situ synchrotron SAXS measurements confirmed that the small spheres assembled quickly and then continued to agglomerate into the larger superstructures during the further course of the reaction. While the high metallic character of the nanoparticles was expected to cause characteristic tin scattering, SAXS and WAXS measurements for those initial materials only showed a correlation length in a range of 1-6 nm that can not yet be assigned with certainty to any material property [4]. Other materials later synthesized under different conditions on the other hand showed signals in the WAXS area that can be assigned to white tin(Figure 2.13). These only appeared in samples that had been prepared without a catalyst. These materials also diplayed a different morphology during SEM measurements, with heaps of irregular shapes instead of spheres (Figure 2.14) [5].

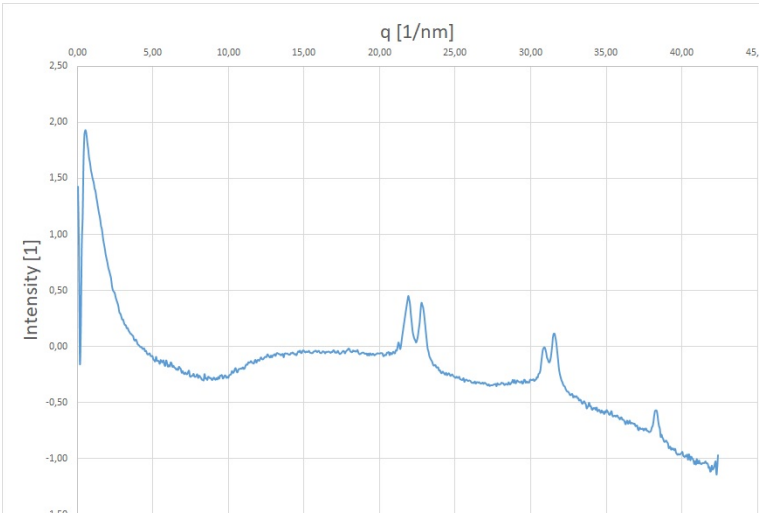

Figure 2.13: WAXS signals of *o*-tolyl@Sn synthesized at RT in benzene without catalyst

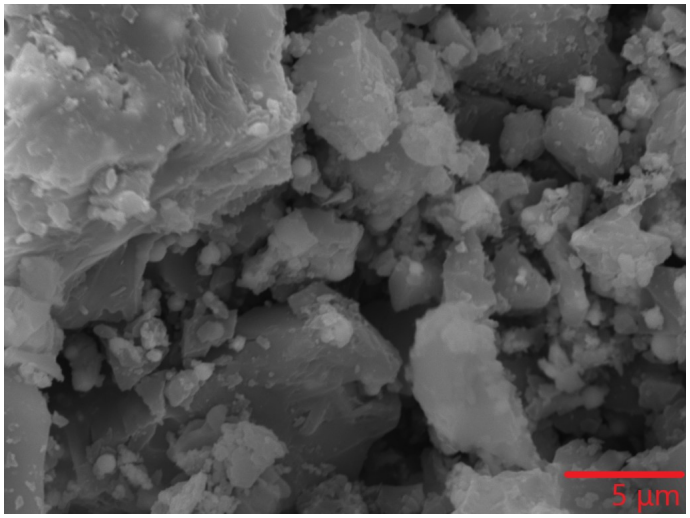

Figure 2.14: Morphology of *o*-tolyl@Sn synthesized at RT in benzene without catalyst under SEM [5]

The conditions leading to the observance of WAXS peaks correlating to white tin such as reaction temperature, presence of catalyst, aryl substituent and solvent have to be further explored and optimized and are the main objectives of this work.

3 Results and Discussion

3.1 Screening of *o*-Tolyl@Sn Nanoparticles

As mentioned before (Chapter 1), aryl@Sn nanoparticles displaying characteristic white tin scattering patterns are indicative of high Sn(0) content in the particle cores and thus a high metallic character. They are consequently the most promising candidates of the arly@Sn type materials for possible electronic applications. In order to better understand the relevant factors in the formation of the metallic core and optimize reaction conditions towards increasing its size, this work screened a variety of materials synthesized under different reaction conditions (Figure 1.1) for their properties. Previous research into this area [5] showed that bigger substituents such as mesityl and naphthyl lead to higher workloads and considerably lower yields during the preparation of the starting material. In addition, the difficulty of removing naphthalene, generated by the cleavage of the substituent during polymerization, from reaction mixtures is well known in chemistry. Due to this and the well established nature of the dehydrogenation reaction with the *o*-tolyl substituent in our working group, $o-\text{tolylSnH}_3$ was chosen as a model compound. The general formula of the reaction is depicted in Figure 3.1 Despite Reischauer's work showing that WAXS signals only occur in materials synthesized without a catalyst [5], every reaction was performed both with and without TMEDA to enable comparisons of the resulting materials. Notably, solvents with electron donor properties, such as Et_2O and DME, are also able to weakly coordinate to the central tin atoms, providing a very slight catalytic effect even in the absence of TMEDA. As discussed in 2.4, reaction progress is indicated by a color change of the mixture. However, this color is only caused by absorption from the particles, the supernatant usually remains colorless, which can be seen upon centrifugation of the mixture. Because the cleavage of not only hydrogen but also organic substituents has been confirmed by both Zeppek [4] and Reischauer [5], the supernatant of the reaction mixtures was not analyzed any further.

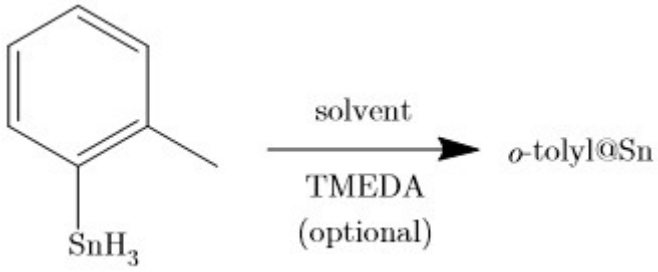

Figure 3.1: General reaction formula of the dehydrogenation of $o-$tolylSnH$_3$

3.1.1 Coupling at Room Temperature

The most basic variant of the reaction involves just stirring the reacting compounds at ambient temperature without additional energy sources.

3.1.1.1 Coupling at Room Temperature without TMEDA

Due to the labile Sn-H bond, this reaction proceeds even without a catalyst, although the aryl ligand serves to stabilize this bond [16, 17] and consequently slows down the reaction to a point were full completion takes several weeks to months. This provided two challenges. The long reaction time significantly increased the danger of air contamination, especially with regular pressure equalization being required due to the H_2 evolution. Special care had to be taken to ensure a fully closed set up with well fitting glass joints and sufficient grease. Moreover, because of the mixtures' black color, the end point of the reaction was difficult to determine. The supernatant did not always lose its color completely. Other times particles were so fine that they stayed dispersed despite centrifugation. Therefore, the bottom of the flasks where checked for deposited solid after centrifugation to provide an additional clue about the reaction end point.

According to expectations, the nanoparticles synthesized without TMEDA showed the characteristic diffraction pattern of β-tin. For measurements taken at a wavelength of 154 nm, the received 2θ angles were 30.52, 31.96, 43.82, 44.84 and 55.24 ° as well as a signal that is hard to make out due to strong background at 62.40 °. This is consistent with the reported scattering patterns for powder X-ray of β-tin [72]. The peaks visible in the area of 10-15 nm^{-1} of compound **(7)** are caused by the foil used for closing the sample holder (more on this in Section 3.3).

In DME as a solvent, synthesis without a catalyst **(8)** was so far unsuccessful. Despite the reaction mixture turning a dark brown quickly, no solid polymeric material formed. After a reaction time of about 2 month, silvery flakes with a metallic sheen which were

inert in air, possibly consisting of pure tin(0) formed. Because of the strong donor properties of the bidentate DME, reactions proceed considerably faster, as previously shown [4, 5], leading to difficulties in isolating the nanoparticles. More research into this is needed. All the other samples behaved as would be expected. Different packing densities of the samples for the scattering experiments explain the different peak and background intensities. There is no apparent solvent effect. The elemental analysis returned 18.6% C and 1.4% H for **(7)**, 9.6% C and 1.5% H for **9** as well as 13.9% C and 1.2% H for **10**. The scattering plots for these compounds are displayed in Figure 3.2, with small red arrows in these and all following X-ray scattering charts denoting the characteristic β-tin scattering signals.

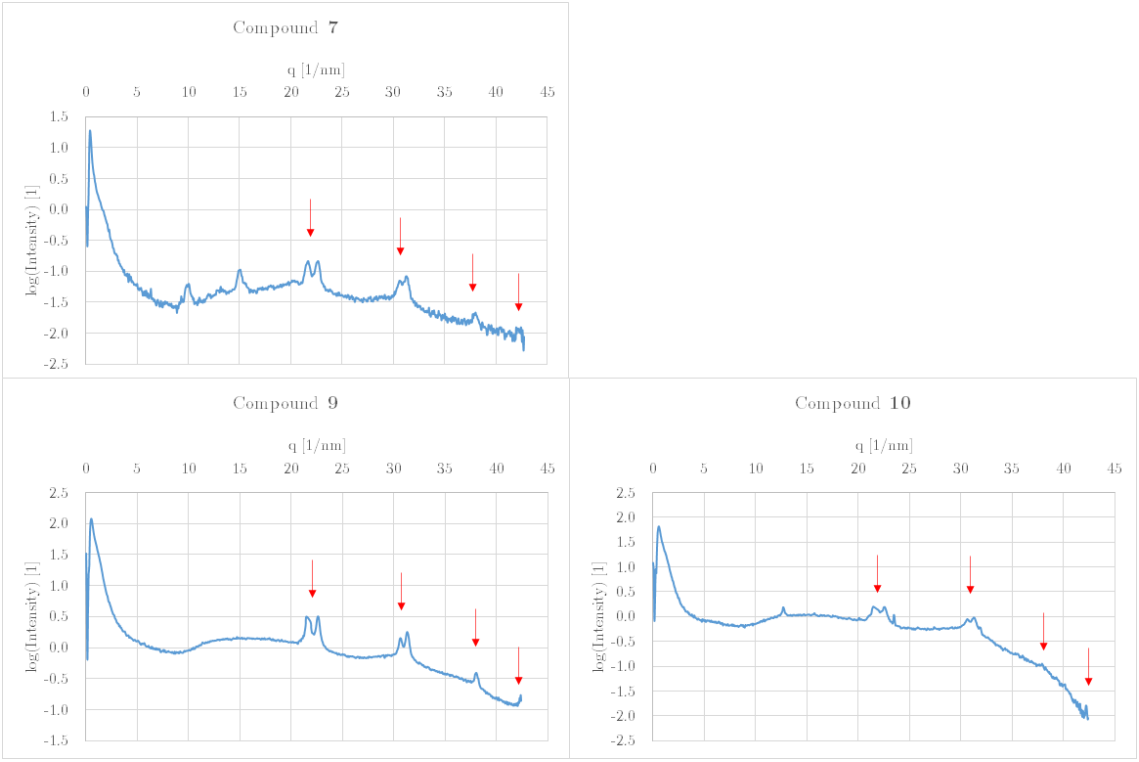

Figure 3.2: X-ray scattering signals of **(7)** (top left), **(9)** (bottom left) and **(10)** (bottom right), *o*-tolyl@Sn synthesized at RT without catalyst in toluene, benzene and cyclohexane, respectively. Red arrows correspond to β-tin scattering signals.

An additional experiment conducted without a solvent or stir bar shows the same scattering behavior without any apparent differences caused by the changes in synthesis procedure. The elemental contents of 18.2% C, 1.7% H are also well in line with expectations. In comparison, Reischauer also found Sn(0) signals for *o*-tolyl@$^{\text{toluene, 25 °C}}$Sn, although the peak intensities are considerably lower than the ones found in this thesis, possibly due to a shortened reaction leaving less time for Sn(0) formation [5].

3.1.1.2 Coupling at Room Temperature with TMEDA

With the addition of a TMEDA catalyst, room temperature reactions become very easy to perform. As they complete in less than an hour and generate high volumes of hydrogen gas, air contamination is not a big concern. With the short reaction time, pressure equalization can be easily performed *via* the schlenk line. However, when X-ray scattering experiments are performed, this materials show something very different from their catalyst free counterparts: They do not display β-tin scattering, allowing instead the determination of a correlation length. Compound **(11)** had a correlation length of 1.7 nm and an elemental composition of 28.0% C and 2.3% H. Figure 3.3 shows its scattering curve in comparison to that of **(7)**, synthesized under the same conditions but without TMEDA. Small yellow arrows in these and all following X-ray scattering charts show the region where the correlation length is determined.

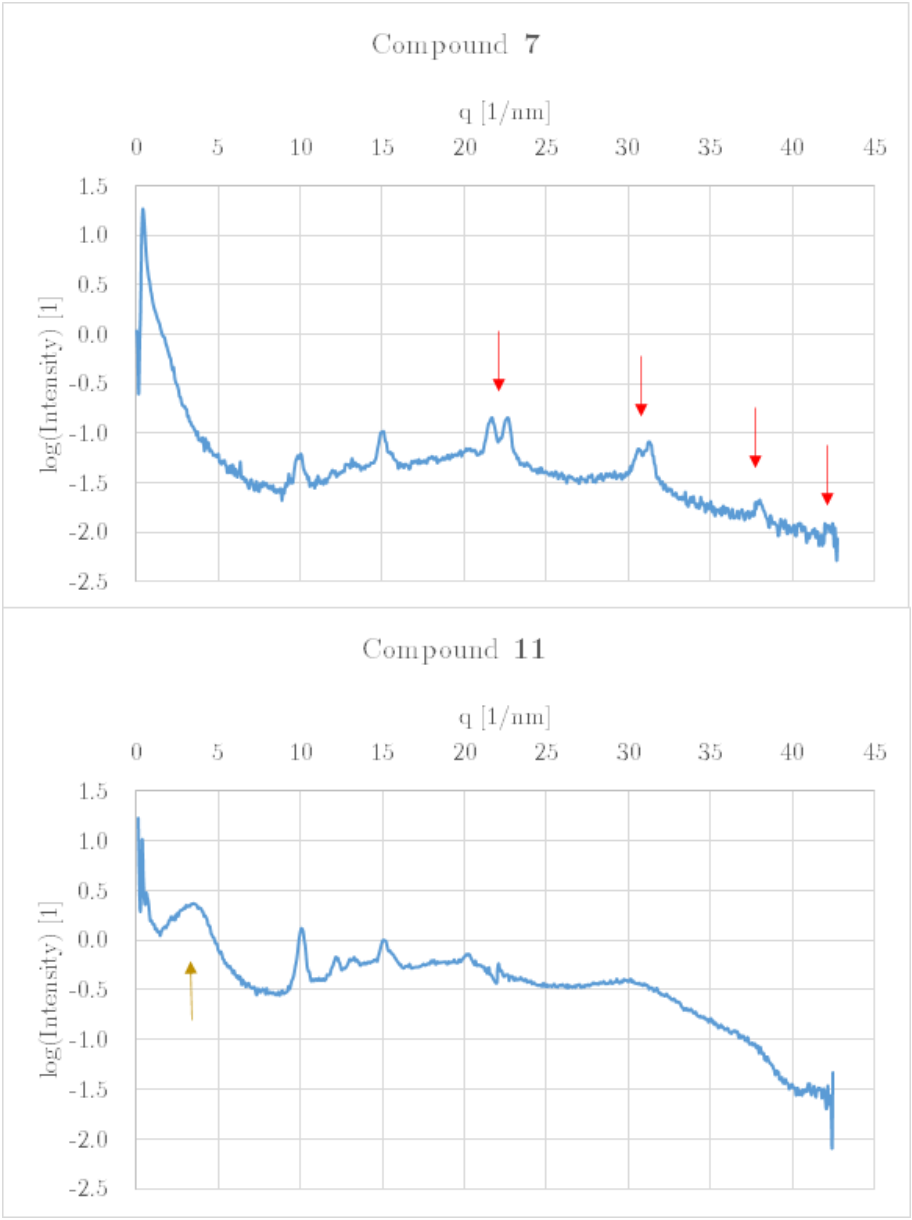

Figure 3.3: Top: X-ray scattering signals of **(7)** Bottom: X-ray scattering signals of **(11)** Red arrows correspond to β-tin scattering signals, the yellow arrow shows the peak for calculation of the correlation length of the micro-morphology.

Compound **(12)** had a correlation length of only 1.4 nm, significantly smaller than that of **(11)**. That might be caused by the higher donating properties of DME compared to toluene, speeding up the reaction and leaving less time for the formation of larger particles. Here the EA returned a carbon content of 30.1% and a hydrogen content of 2.4%. The scattering plot can be seen in Figure 3.4, with no comparison to its TMEDA free counterpart available because the synthesis of **(8)** was not succesful.

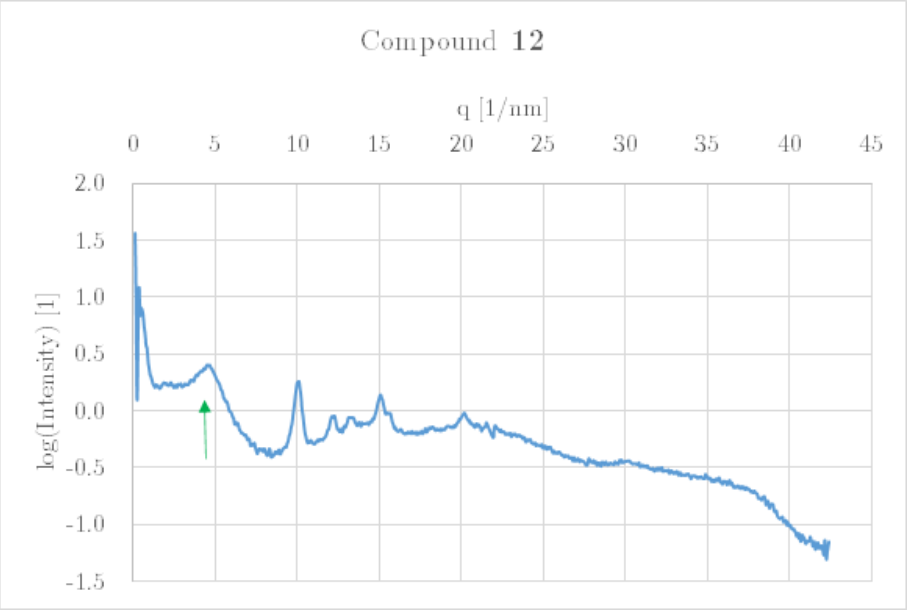

Figure 3.4: X-ray scattering signals of **(12)** The yellow arrow shows the peak for calculation of the correlation length of the micro-morphology.

The correlation length of **(13)** was longer again with 1.7 nm, supporting the theory that it is affected by solvent polarity. The same trend was already observed by Zeppek, who measured very similar values (1.7 nm in toluene, 1.5 nm in DME and 1.8 nm in cyclohexane)[4]. It had 22.6% C and 2.2% H. Figure 3.5 shows the scattering plot in comparison to **(9)**.

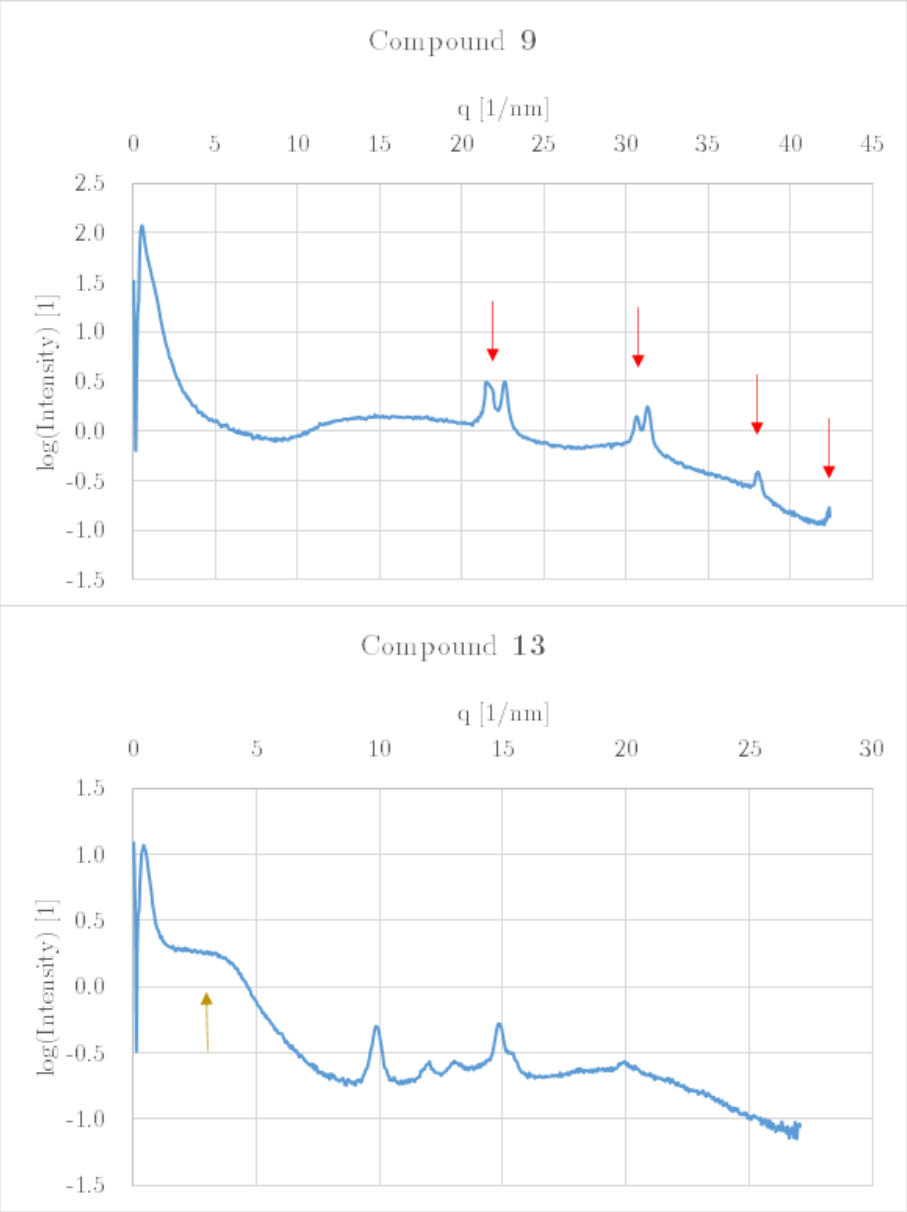

Figure 3.5: Top: X-ray scattering signals of **(9)** Bottom: X-ray scattering signals of **(13)** Red arrows correspond to β-tin scattering signals, the yellow arrow shows the peak for calculation of the correlation length of the micro-morphology.

A very unexpected result occurred in the first batch of a sample synthesized with cycohexane as a solvent, compound **(14)**-1. Despite the use of TMEDA as a catalyst, the scattering experiment displayed characteristic tin reflections. A correlation length might also be present but its peak does not protrude from the background enough to allow its determination. The same result also occurred in another sample synthesized in cyclohexane at 50 °C (see Section 3.1.2). A so far inexplicable interaction with the solvent might be the key to an explanation. Unfortunately, the result was not reproducible in a

second batch of material synthesized under the same reaction conditions, compound **(14)**-2. It displayed instead a correlation length, which was 1.8 nm, although the measurement had an uncharacteristically strong background. Some form of contamination might explain why it showed a different result. Aryl@Sn nanoparticles synthesized in cyclohexane should be investigated further, for they might provide a way towards material with a high metallic character with very short reaction times. Both **(14)**-1 and **(14)**-2 are displayed in Figure 3.6 alongside a comparison to **(10)**.

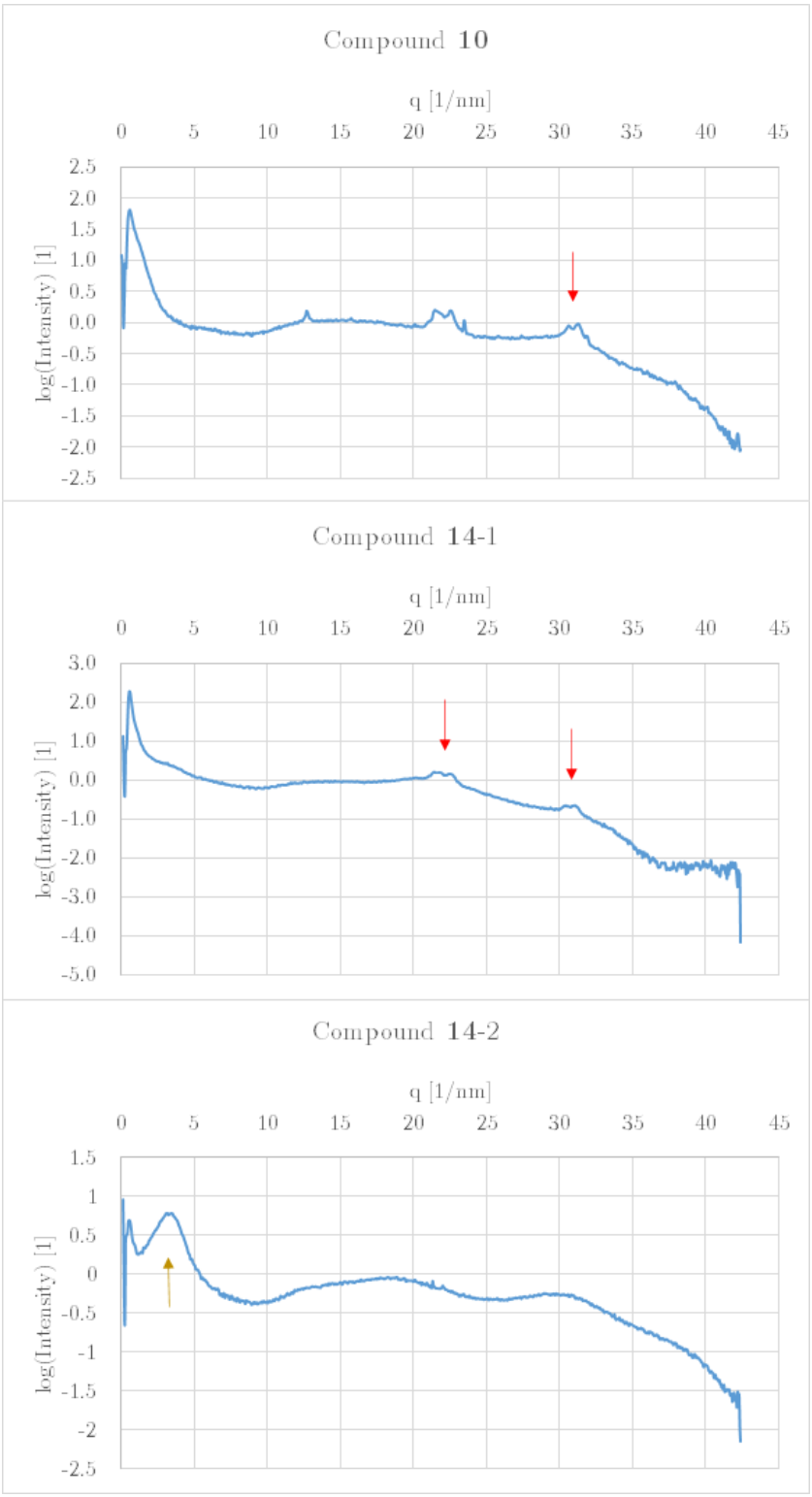

Figure 3.6: Top: X-ray scattering signals of **(10)** Middle: X-ray scattering signals of **(14)**-1 Bottom: X-ray scattering signals of **(14)**-2 Red arrows correspond to β-tin scattering signals, the yellow arrow shows the peak for calculation of the correlation length of the micro-morphology.

3.1.2 Coupling at Elevated Temperatures

These reactions were carried out at temperatures of around 50 °C in order to study the effects of elevated temperatures on the properties of the resulting materials and to potentially speed up nanoparticle formation.

3.1.2.1 Coupling at Elevated Temperatures without TMEDA

Although the higher temperature serves to speed up the reactions, they still require around a week for completion. In addition to that, the heating increases the pressure developing in the reaction vessel. Because using a bubbler and a N_2 or Ar stream for the entire duration would be inefficient, it was initially attempted to protect the reaction with a gas reservoir closed by a paraffin oil reservoir. However, for efficiency, the setup was switched to a closed flask with pressure equalization carried out manually once per day *via* the schlenk line.

Contrary to expectations, **(15)** did not show Sn(0) signals. Neither did it show any correlation length, a result consistent with degraded samples, the most likely explanation being air contamination and ensuing oxidation at some point in the process. The EA shows 15.0% C and 1.2% H. The EA for **(16)** returned 28.2% C, 2.3% H. It once again has the signals from β-tin. In addition to that, additional signals appear in the form of a singlet at 6.2 nm^{-1}, a duplet at 7.6 nm^{-1} and a triplet at 12.8 nm^{-1}, in addition to a strong background. These additional signals appear to be characteristic for materials synthesized at elevated temperature without catalyst (**16**-**18**), but not in the samples synthesized with a catalyst (**19**-**22**). The cause is not yet known. Possibly the high temperatures result in the formation of different kinds of agglomerates. Unfortunately, only one specimen from this category, **(18)**-1, had enough material left over to prepare a sample. As described in more detail in 3.6, in addition to the expected nanoparticles, there were indeed needle like structures visible under the SEM (see Figure 3.19) that were not present in any of the other SEM samples. Compound **(17)** possibly shows Sn(0) scattering, but the background is too strong and the peak intensities are too low to say so with certainty. Also, no sensible elemental analysis could be performed either due to high sample heterogeneity and the material should therefore be prepared again to provide a better basis for analysis. Two batches were synthesized of **(18)**, **(18)**-1 and **(18)**-2, because the first displayed an uncharacteristic grey color instead of the usual black and a slight tin mirror had developed on the flask wall. SAXS/WAXS analysis displayed Sn(0) scattering which could be indicative of both nanoparticles with high metallic character as well as elemental tin. However, the EA showed a composition of 23.6% C and 2.1% H, in line with the organic content of nanoparticles, indicating that

the material is indeed not just tin. The second batch had very low scattering intensities. The elemental analysis showed 42.4% C, 3.7% H for **(18)**-2, which is higher than the organic content of the starting materials and thus either caused by heavy contamination or an analysis error, but a third batch was not prepared because elemental analysis had confirmed the identity of **(18)**-1 as nanoparticles. Figure 3.7 shows the various scattering plots, excluding **(19)**-2 due to the bad condition of the material. The black asterisks denote the additional peaks in the WAXS range.

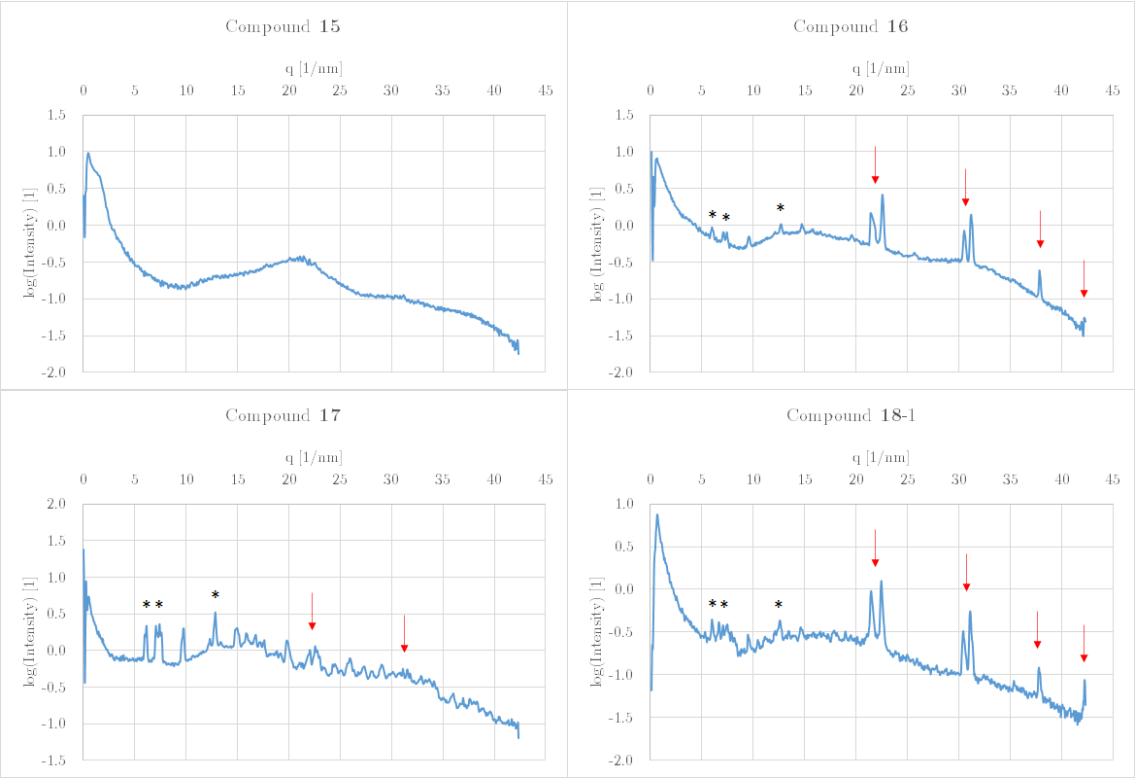

Figure 3.7: X-ray scattering signals of **(15)** (top left), **(16)** (top right)**(17)** (bottom left) and **(18)** (bottom right), *o*-tolyl@Sn synthesized at 50 °C without catalyst in toluene, DME, benzene and cyclohexane, respectively. Red arrows correspond to β-tin scattering signals, black asterisks denote additional unexpected WAXS signals.

In contrast to the reactions at elevated temperature without TMEDA in this work, **(15-(18)**, Reischauer was able to find a correlation length of 3.3 nm for *o*-tolyl@$^{Et_2O,\ reflux}$ but not characteristic peaks in the WAXS region [73], possibly due to a shortened reaction time of only 72 h, not leaving enough time for the metallic core to form. The comparability for these materials is limited because the low boiling point of 34.6 °C did not allow the same elevated temperatures of 50 °C as in other samples to be reached.

3.1.2.2 Coupling at Elevated Temperatures with TMEDA

The challenge here was to ensure a constant reaction temperature while at the same time preventing solvent from evaporating and changing the concentration. Therefore both solvent and starting material were heated to the desired temperature, then TMEDA added through the reflux condenser. Compound **(19)** has a correlation length of 1.9 nm and consists of 24.6% C and 2.1% H. Its scattering plot is shown in Figure 3.8. The counterpart without TMEDA is not shown here because it did not display any scattering signals. However, the same material synthesized at room temperature, **(11)** is added for comparison of temperature effects, whith higher temperature seemingly resulting in increased correlation length.

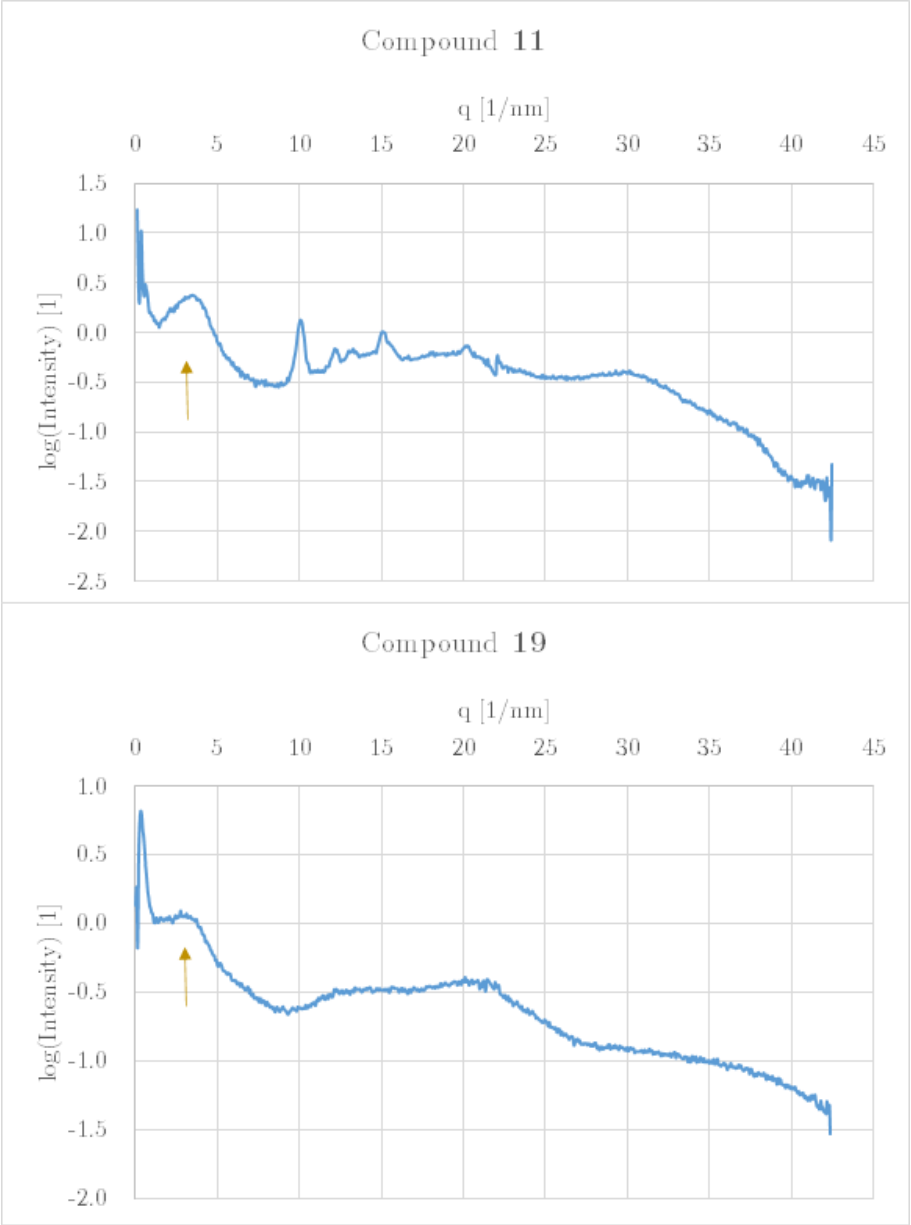

Figure 3.8: Top: X-ray scattering signals of **(11)** Bottom: X-ray scattering signals of **(19)** Yellow arrows show the peak for calculation of the correlation length of the micro-morphology.

The correlation length for **(20)** is 1.5 nm, with a composition of 30.2% C and 2.7% H. It is displayed, alongside its counterpart synthesized at elevated temperature without TMEDA, in Figure 3.9. Notably, the maximum q value for **(20)** is lower than in most other scattering experiments. This is due to a different measurement procedure that was tried out but subsequently abandoned because it cuts off some of the characteristic β-tin scattering signals.

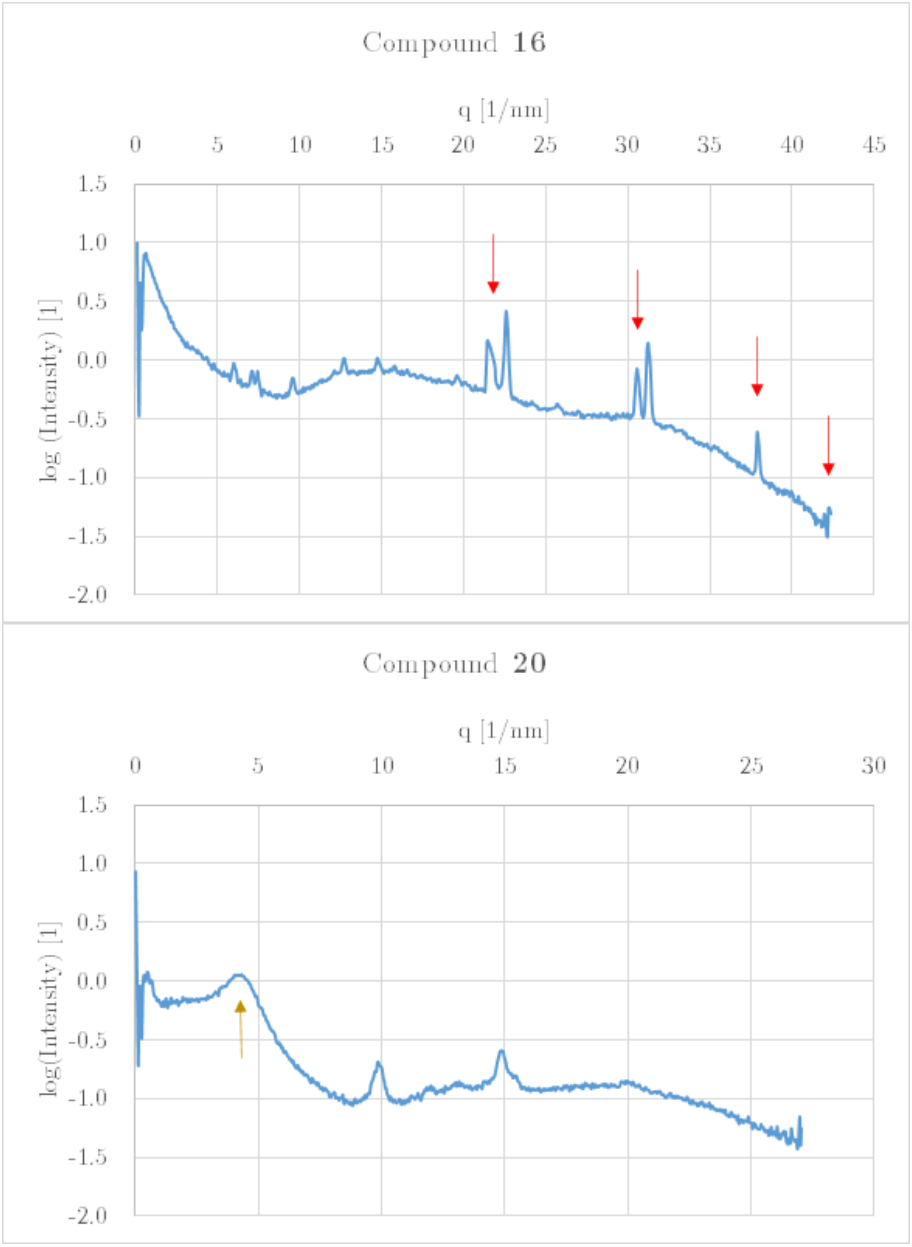

Figure 3.9: Top: X-ray scattering signals of **(16)** Bottom: X-ray scattering signals of **(20)** Red arrows correspond to β-tin scattering signals, the yellow arrow shows the peak for calculation of the correlation length of the micro-morphology.

Compound **21** has a correlation length of 1.7 nm, a carbon content of 26.0% and a hydrogen content of 2.4%. It is shown alongside **(17)** in Figure 3.10.

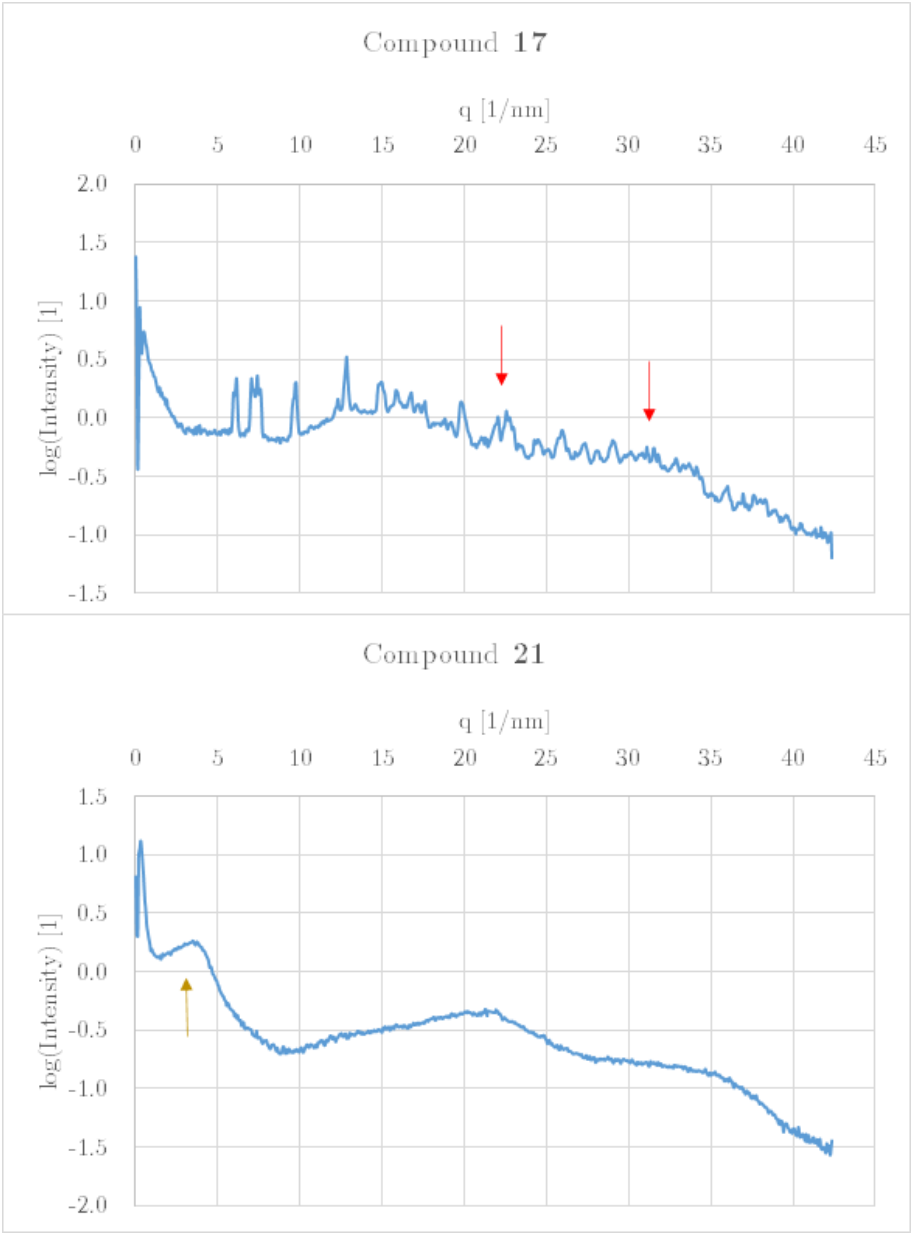

Figure 3.10: Top: X-ray scattering signals of **(17)** Bottom: X-ray scattering signals of **(21)** Red arrows correspond to β-tin scattering signals, the yellow arrow shows the peak for calculation of the correlation length of the micro-morphology.

Compound **22** once again displayed unexpected Sn(0) scattering with low intensity similarly to **14**-1 despite being synthesized with a catalyst. In addition to that, however, the hump caused by the correlation length is big enough here to calculate it at 2.2 nm. This suggests that an intermediate between the two types of nanoparticles with high and low metallic character is present. EA returned 14.9% C and 1.4% H. Figure 3.11 shows it alongside **(18)**-1.

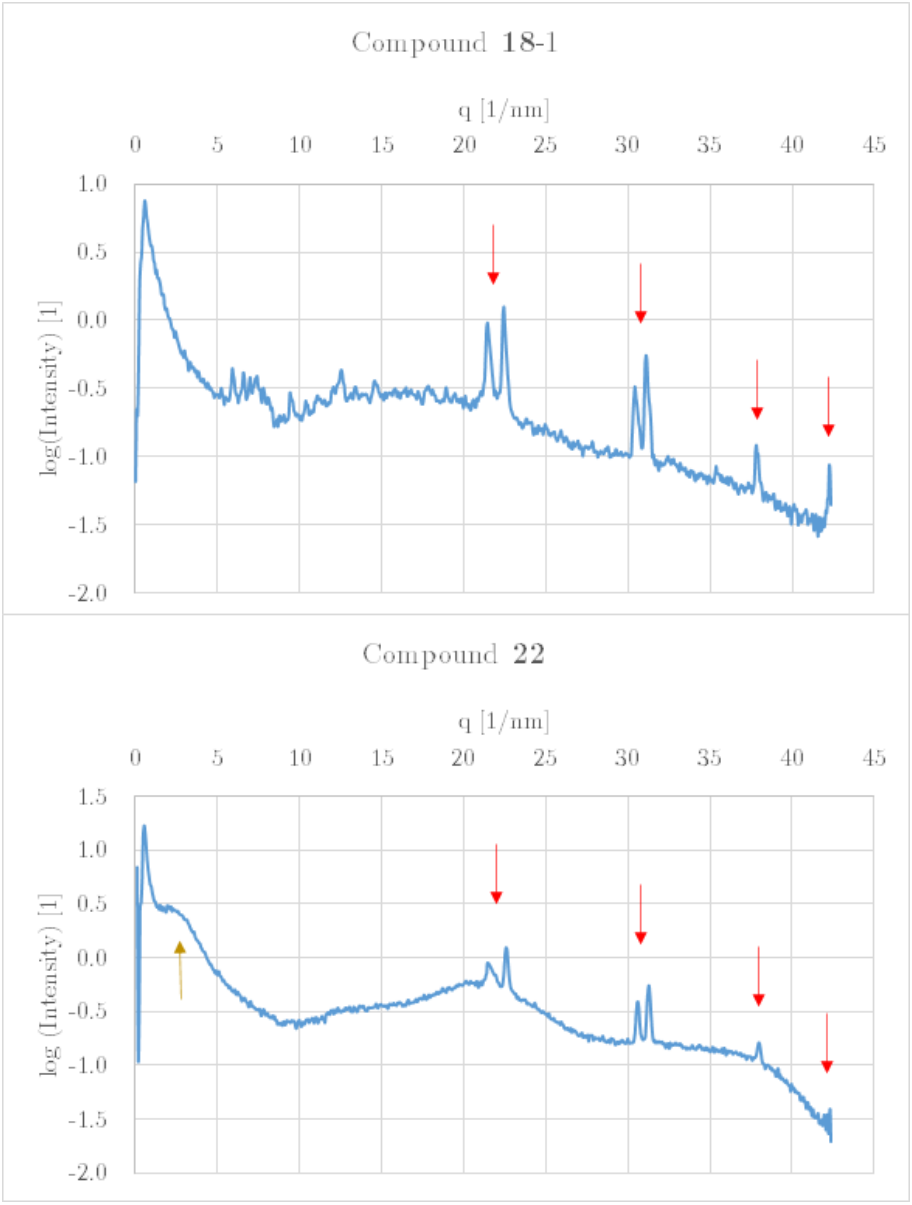

Figure 3.11: Top: X-ray scattering signals of **(18)** Bottom: X-ray scattering signals of **(22)** Red arrows correspond to β-tin scattering signals, the yellow arrow shows the peak for calculation of the correlation length of the micro-morphology.

3.1.3 Ultrasonication Assisted Coupling

The long runtime of catalyst free reactions also posed challenges in combination with ultrasonication. Because of noise concerns, the sonication bath could not be placed next to the schlenk line. Samples thus had to be removed from the bath and carried through several rooms for pressure equalization. Because of the heat development, constant cooling of the sonication bath had to be ensured as well and the bath water regularly

topped off. The general setup is shown in Figure 3.12. In addition to that, the formation of a grey shroud on the walls of the reaction flasks could be observed after only a few days in every reaction. The stress induced by the sonication might cause degradation of the educt, resulting in the formation of elemental tin in addition to nanoparticles. Taken together, these challenges could not so far be overcome and no materials from a catalyst free sonication assisted synthesis are available. With the inclusion of TMEDA, correlation lengths of 1.5 nm in toluene (compound **23**), 1.5 nm in DME (compound **24**), 1.7 nm in benzene (compound **25**) and 1.8 nm in cyclohexane (compound **26**) were found, very similar to those observed at room temperature without sonication. Reischauer previously discovered morphological differences in sonicated samples [5], but only at the μm scale, which would not be detectable using SAXS. The elemental compositions are 23.8% C, 2.9% H for **23**, 36.5% C, 3.3% H for **(24)**, 32.5% C, 3.3% H for **25** and 26.0% C, 2.7% H for **26**.

Figure 3.12: Setup of the sonication bath with external cooling coils

3.2 Screening of 1-Naphthyl@Sn Nanoparticles

Synthesizing the educt 1-naphthylSnH_3 is a more time consuming process with lower yields than for the *o*-tolyl substituent. There are a couple of reasons for this. The naphthyl substituent is cleaved from the tin more easily than the tolyl one, causing higher losses during the reaction. Moreover, the resulting naphthalene is a sublimable solid and the difficulties of removing it from reaction mixtures are well known in chemistry, even more so under inert conditions. Finally, the grignard reagent naphthyl-Mg-Sn solidifies upon cooling down, severely complicating transference onto the $SnCl_4$ and requiring far greater amounts of solvent to be used. Due to this and problems in the workup [5], that compound was not the main focus of this work. However, four preliminary experiments with the naphthyl residue were carried out at room temperature with TMEDA with to allow some basic investigations of substituent influence. Correlation length of 1.7

nm for **27**, 1.6 nm for **28**, 1.7 nm for **29** and 1.7 nm for **30** were found. The SAXS plots are displayed in Figure 3.13. The correlation lengths are well in line with the results found for an *o*-tolyl substituent. One difference is somewhat sharper peaks for 1-naphthyl@Sn, indicating a more narrow distribution in correlation length. Notably, none of the previously reported [5] characteristic naphthalene scattering was found here. This might indicate that the new removal procedure for naphthalene under reduced pressure was at least partially successful, opening up the materials for SEM investigations.

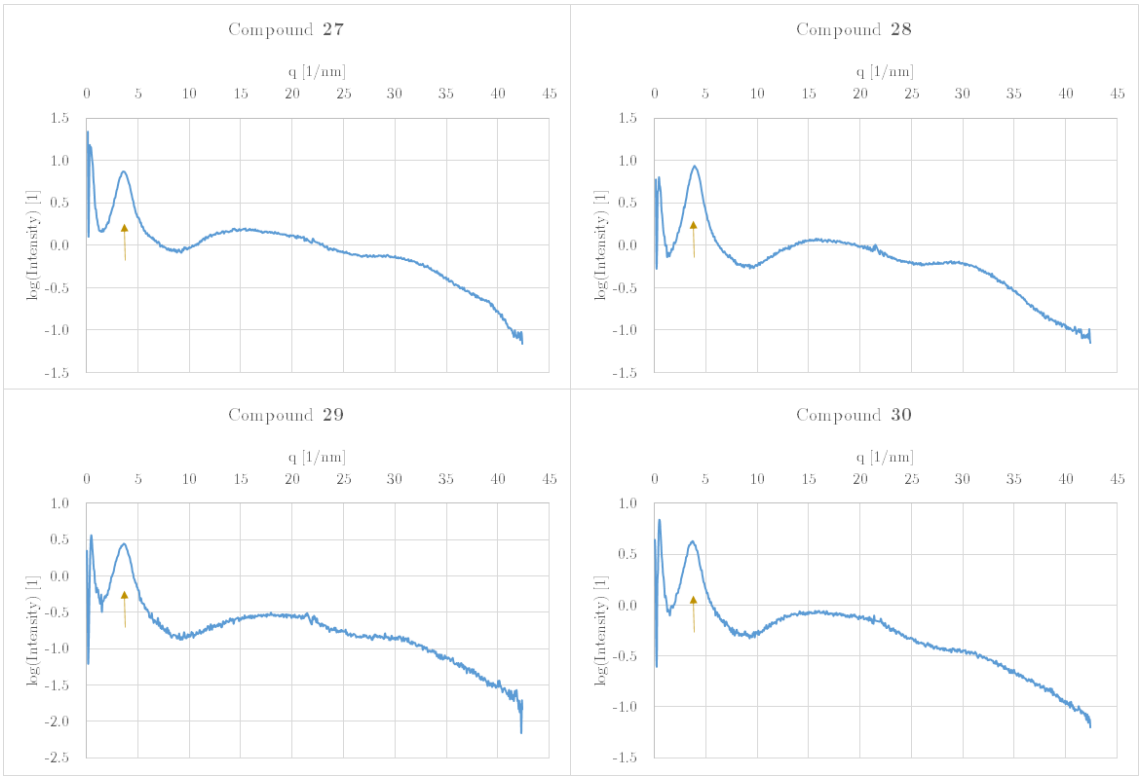

Figure 3.13: X-ray scattering signals of **(27)** (top left), **(28)** (top right)**(29)** (bottom left) and **(30)** (bottom right), 1-naphthyl@Sn synthesized under sonication with TMEDA in toluene, DME, benzene and cyclohexane, respectively Yellow arrows show the peak for calculation of the correlation length of the micro-morphology.

3.3 Developing a New SAXS Procedure Suitable for Screening Processes

The preparation of a sample for SAXS measurements is a time and work intensive process. Because of their air sensitivity, all samples are stored in the glove box. The sample holder has to be introduced into the glove box. Next the electrostatic powder has to be transferred into the holder, covered with a thin foil and the holder has to be screwed

shut. For transportation from the glovebox to the SAXS-device it has to be put into a bigger, inert container.

Previously, a stage able to incorporate a single powder sample was employed for SAXS measurements. Due to the higher amount of samples generated for screening purposes in this work, this process did not seem suitable. Thus, a newly received sample stage (Anton Paar GmbH) able to host 4x5 samples at the same time was used (Figure 3.14). Charging it with multiple samples at a time greatly reduced the time and effort for transference to and from the glove box as well as assembly. As can be seen in Figure 3.15, adhesive type is required to enclose the samples in the stage. A broad tape from TESA® was initially used to cover the entire sample stage at once. However, this tape turned out to cause scattering peaks in the WAXS area during blank measurements, reducing the measurement quality with its strong background (see for example the plot of **(7)** in Figure 3.2). For this reasons the TESA® tape was replaced with one manufactured by Scotch®, significantly smaller and only able to cover a single column or row of samples at a time, as shown in Figure 3.15. After removal from the glove box, the stage was placed in an argon filled bucket, brought to the SAXS device and measured.

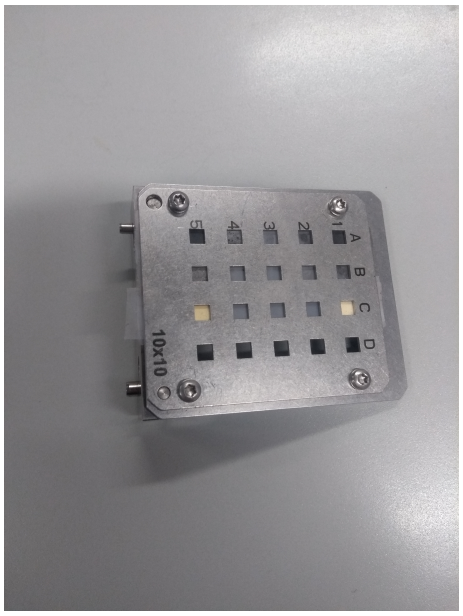

Figure 3.14: The assembled multi-sample stage for scattering measurements

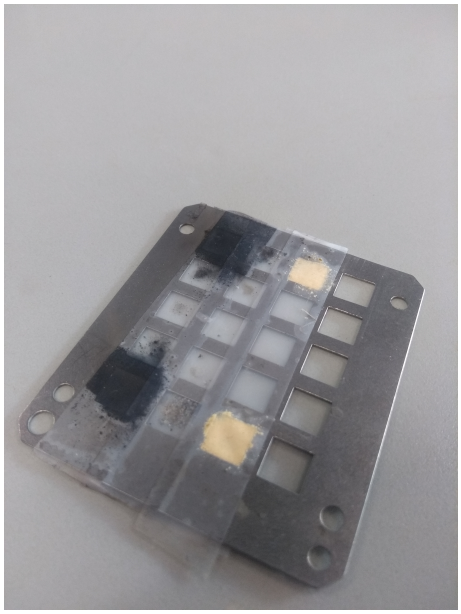

Figure 3.15: The inner part of the disassembled SAXS sample stage

Another time consuming part of these measurements was manually readjusting the position of the stage for each individual sample. An automatic procedure for screening processes was included in the control program of the SAXS device, however it did unfortunately not fit the dimensions of the sample holder. The relative position of each individual sample was therefore determined using sweeps over the entire stage and measuring beam transmission. An automatic procedure for multiple measurements at the predetermined positions was then employed.

3.4 Confirmation of Sn(0) Presence Using Powder XRD

For inert powder XRD, micro capillaries would have to be filled with the inert powder inside the glove box, then the capillaries molten closed and transferred to the powder XRD machine. Unfortunately, the individual powder particles proved too large to fit inside the capillary. Due to the low amounts of material, no mortar could be employed for decreasing its size, not enough material would be left after the losses. The process was further complicated by the electrostatic nature of the nanoparticle powder. Thus, no successful XRD measurement could be performed yet. Future attempts will involve forcing the material into the capillary through use of a thin wire and, as a last resort, synthesizing a big batch of material that can be pulverized very finely in a mortar.

3.5 Elementary Analysis of Synthesized Compounds

The elementary analysis determines the percentage of carbon and hydrogen in a sample, thus showing the remaining organic content. Because the organic content is expected to correlate with the metallic character of the nanoparticles, elementary analysis is a key aspect in the characterization of these materials. Although the elementary compositions have already been provided alongside each individual compound in Sections 3.1 and 3.2, they are all summarized in Table 3.1 to provide a better overview. When comparing the substances, it becomes apparent that on average, the catalyst free variants have less organic content than their counterparts. This is very much in line with expectations based on the theory of additional organic residues getting cleaved over longer reaction times. The cleaved residues are removed from the sample under reduced pressure, thus increasing the tin content. Similarly, those samples synthesized in the donating DME always have the highest organic content whereas those from the very apolar cyclohexane tend to have the lowest, also indicating a longer reaction time with additional residue cleavage. One sample, **18**-2, has a higher carbon content than the starting material which is inconsistent with the synthetic procedure. Either a measurement error occurred or the sample was contaminated at some point.
The 1-naphthyl-samples have higher residual organic content than the *o*-tolyl-samples. Because the sterically more demanding naphthyl substituent is expected to be less stable, it is unlikely that less cleavage occurs. It stands to reason that, despite there not being corresponding signals in the WAXS range, cleaved naphthalene was not succesfully removed from the sample. A SEM analysis could confirm whether that is indeed the case.

Compound	C [%]	H [%]
$o-$tolylSnH$_3$	39.5	4.7
(o-tolylSn)$_n$	40.1	3.4
7	18.6	1.4
9	9.6	1.5
10	13.9	1.2
11	28.0	1.4
12	30.1	2.4
13	22.6	2.2
14-1	20.0	1.3
14-2	26.9	2.6
15	15.0	1.2
16	28.2	2.3
18-1	23.6	2.1
18-2	42.4	3.7
19	24.6	2.1
20	30.2	2.7
21	26.0	2.4
22	14.9	1.4
23	32.8	2.9
24	36.5	3.3
25	32.5	3.3
26	26.0	2.7
1-naphthylSnH$_3$	48.3	4.1
1-naphthylSn$_n$	48.9	2.9
27	39.8	2.4
28	45.9	2.6
29	41.8	2.5
30	37.8	2.3

Table 3.1: C and H content of synthesized compounds as determined by EA

3.6 Scanning Electron Microscopy

Due to logistical constraints, only a small number of the available samples could be analyzed under the SEM. Unfortunately, the measurement procedure required a short exposure of the samples to ambient air. Due to their high sensitivity to oxygen, some degradation could not be ruled out. A small amount of one material, **24**, was therefore intentionally oxidized and measured along the others as a blank. In addition, all samples were screened for the presence of oxygen using EDX. Unfortunately, it became immediately apparent, that all samples contained oxygen, with 34% atomic in the intentionally oxidized one, 24% atomic in the same material not exposed to air intentionally and between 30

and 50% atomic in the other samples. Because the EDX results showed a very high variance, the exact amount of oxygen and mass relations to other atoms should not be overinterpreted.

Both the intentionally oxidized sample and the one kept under inert conditions as much as possible of *o*-tolyl@$^{\text{DME, TMEDA, son.}}$Sn **(24)** show an identical structure of very regular, small spheres with a diameter of about 2-3 μm, as seen in Figure 3.16. This morphology is consistent with earlier findings [4, 5] for nanoparticles synthesized in a polar solvent with the addition of TMEDA. These materials also display a peak for the correlation length (1.5 nm) in the small angle region of scattering experiments. Due to the identical nature of both samples and their similarity to previous results [4, 5], it can be reasoned that oxidation does not affect the microstructure of the nanoparticles.

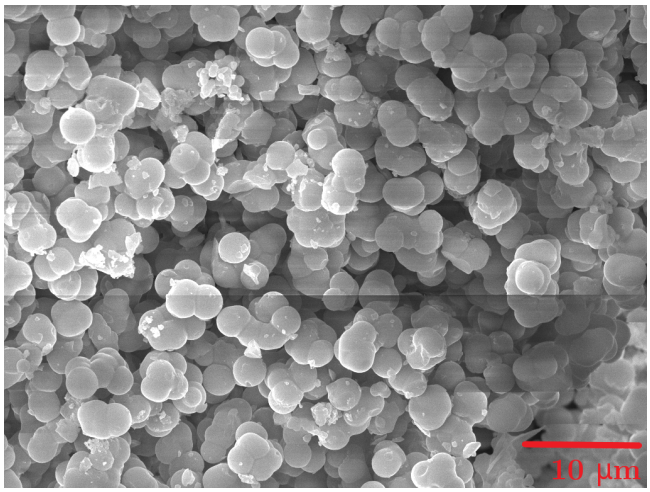

Figure 3.16: SEM picture of **(24)**, intentionally oxidized

When a very apolar solvent is used alongside the TMEDA catalyst, as was the case for *o*-tolyl@$^{\text{cyclohexane, TMEDA, 50 °C}}$Sn **(22)**, a compound with the characteristics of both nanoparticles with a high metallic character and those with a low metallic character is the result: The SEM picture shows some spheres which are very similar to those of **24**. However, the sample is much more heterogeneous. There are also many spheres present which are considerably smaller, down to structures with diameters below 100 nm, the shape of which cannot be made out anymore. The smaller the structures, the more they seem to cling together, aggregating again into heaps of substance. The structure can be seen in Figure 3.17. This mixture of larger and smaller structures might be the explanation for why these specific particles, synthesized in cyclohexane but with TMEDA, displayed both a peak associated with the correlation length and β-tin scattering during the SAXS/WAXS analysis (Figure 3.7). It might be that the very apolar, non-donating

cyclohexane solvent hinders the material formation process and pushes it more in the direction of a catalyst free synthesis.

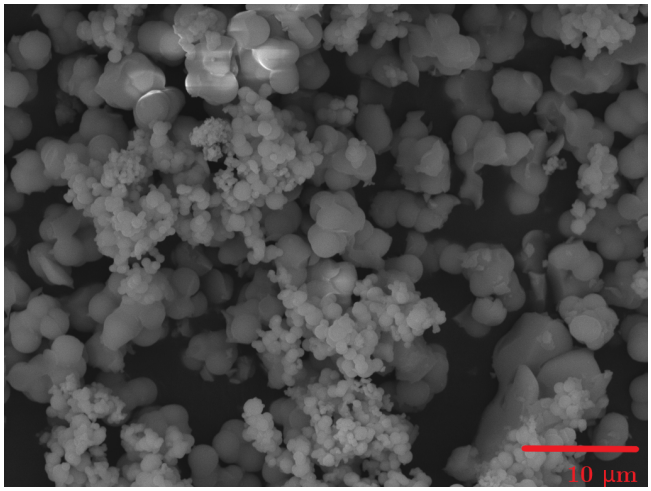

Figure 3.17: SEM picture of **(22)**

Slowing down the reaction even further through removal of the TMEDA catalyst results in nanoparticles which only show the characteristics of a high metallic character. This is illustrated by *o*-tolyl@$^{\text{benzene}}$Sn **(9)**. While a very small number of larger, spherical shapes is still present, even those are considerably smaller than in previous samples, with diameters below 1 μm. The bulk of the material, however, consists of the tiny particles with indiscernible shape, clinging even more tightly together this time to form larger heaps and blocks, see Figure 3.18. This is consistent with previous findings [5] that show a catalyst free synthesis leading to irregular stacks instead of spheres. It is also confirmed by the findings of the WAXS analysis, which displayed characteristic β-tin scattering but no correlation length for this compound (Figure 3.2).

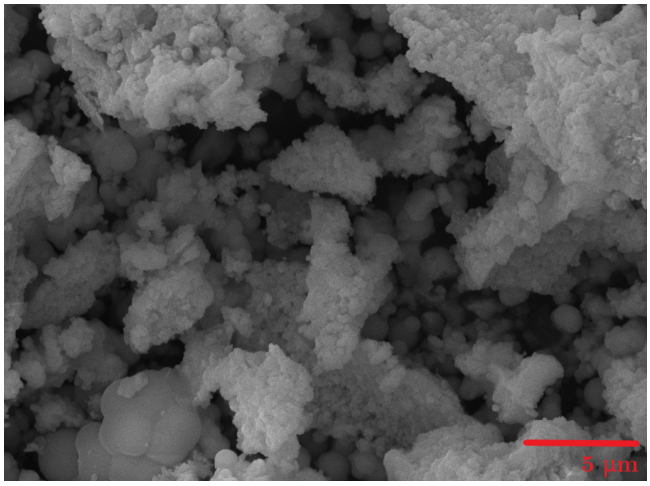

Figure 3.18: SEM picture of **(9)**

The material *o*-tolyl@$^{\text{cyclohexane, 50 °C}}$Sn (**18**-1) looks initially similar to **(9)**, as could be expected, since both samples were synthesized in a non-polar solvent without TMEDA. There is, however, one irregularity: Throughout the sample, large needle like structures are present, as can be seen in Figure 3.19. One possibility is that they are of a contaminant nature, such as stray glass splinters. However, as mentioned previously in section 3.1.2, all samples synthesized at elevated temperatures also displayed unexpected peaks in the WAXS area (compare Figure 3.7), indicating one or more additional crystalline substances of unexplained nature. These two phenomena might be related. In that case, the origin of these rods would have to lie somewhere in the synthesis process at elevated temperatures. SEM analysis of other high temperature samples could confirm this suspicion and open them up for further investigation.

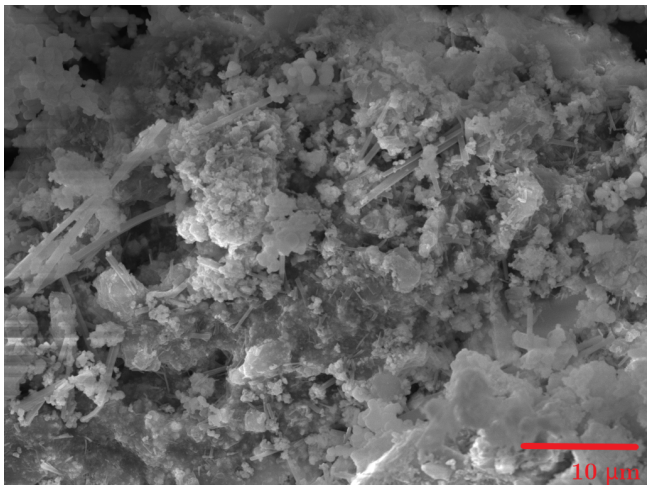

Figure 3.19: SEM picture of **(18)**-1

For *o*-tolyl@$^{\text{toluene, TMEDA}}$Sn **(11)**, SEM was performed half a year after the product was isolated. While initial SAXS measurements (Figure 3.3) showed a peak in the small angle region consistent with samples synthesized in the presence of TMEDA, a second scattering experiment performed close to the time of the SEM measurement showed characteristic β-tin scattering in the WAXS region instead (Figure 3.21), characteristic for samples synthesized in the absence of TMEDA. Compound **11** seemingly underwent further Sn-Sn coupling in the period between initial material formation and the most recent measurements, leading to this change in scattering behavior. Consistent with that, the SEM picture (Figure 3.20) shows small, irregular shapes more similar to the morphology of nanoparticles with high metallic character like **9** than to that of nanoparticles with low metallic character **24**.

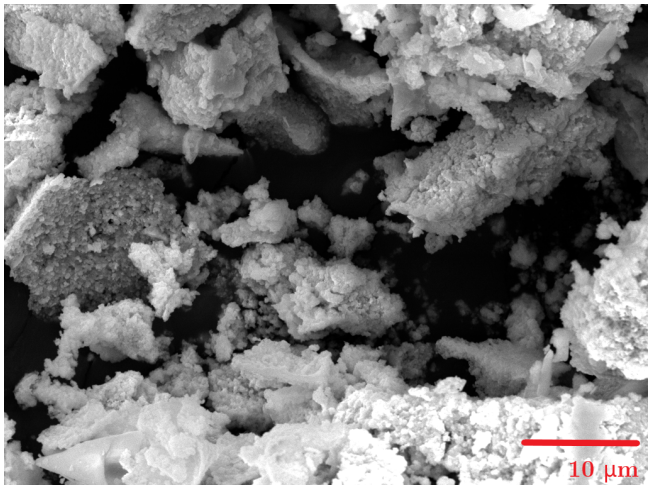

Figure 3.20: SEM picture of **(11)**

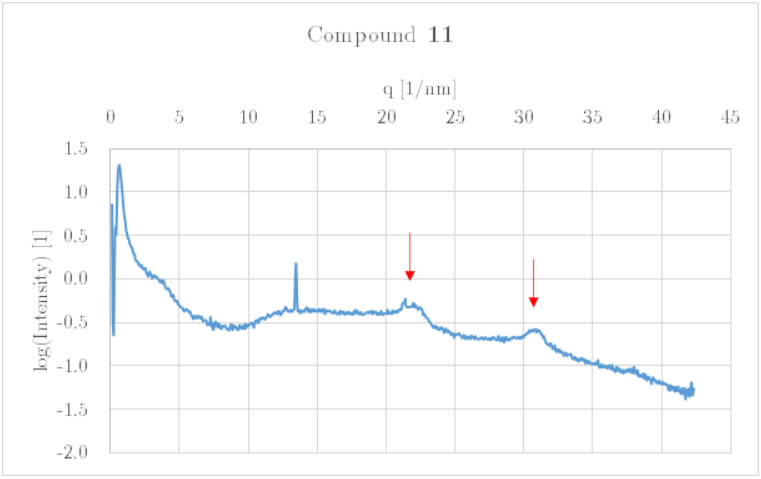

Figure 3.21: X-ray scattering signals of **11**, taken half a year after product isolation. Red arrows correspond to β-tin scattering signals.

4 Conclusion and Outlook

Various Sn polymerization reactions with aryl tin trihydrides were performed. The influences of the following conditions were evaluated: The presence or absence of the amine base catalyst TMEDA, the solvent effect of toluene, DME, benzene and cyclohexane, the differences between reactions run at room temperature and at 50 °C as well as the influence of ultra sonication.

Of the investigated conditions, TMEDA had by far the greatest observable effect on the reaction, as evidenced by comparing the samples synthesized under the influence of TMEDA, **11-14** and **19-30**, to those from a catalyst free process, **7-10** and **15-18**. While the former allow the determination of a correlation length from X-ray scattering experiments, the latter have a greater metallic character, evident in the characteristic X-ray scattering pattern of β-tin that they display. Additionally, the morphology is completely different. Samples synthesized in the presence of TMEDA organize into very regular, comparably large spheres, whereas a slower synthetic process without a catalyst yields smaller, irregular shapes that tend to agglomerate. The higher metallic character of samples from a TMEDA free synthetic process is further shown by elemental analysis: They contain, on average, significantly lower amounts of organic materials than their counterparts produced in the presence of TMEDA.

The donicity of the used solvent seems to have, for the most part, a much weaker effect, only slightly changing the correlation length. No matter whether at room temperature, 50 °C, or under the influence of sonication, nanoparticles synthesized in DME always have a shorter correlation length than their counterparts in toluene, benzene or cyclohexane, confirming previous findings [4]. Similarly, samples synthesized in DME tend to have the highest residual organic content, whereas those synthesized in cyclohexane tend to have the lowest. Because donating solvents also coordinate to the tin atom and thus elongate the Sn-H bond, the dehydrogenation proceeds faster, leaving less time for additional cleavage of Sn-C bonds. The tin atoms remain more sterically shielded and the clusters cannot grow to the same size. This led to interesting results for two samples synthesized in the very apolar cyclohexane with TMEDA: Scattering experiments showed characteristic β-tin peaks in the wide angle region. Compound **22** even displayed both Sn(0) scattering and a correlation length, which, at 2.2 nm, is with some distance the

largest of any of the screened compounds. SEM also showed this compound to look more like a mixture of materials with a high and with a low metallic character, rather than an intermediate, with both bigger, more regular spheres and smaller shapes being present. This compound is possibly an intermediate between nanoparticles with high and with low metallic character. Should that be the case it also offers an explanation why no correlation length can be determined for nanoparticles with a high metallic character: The correlation length is too big, and the scattering signal it causes overlaps with the peak caused by large particle scattering. Indeed, when comparing the SAXS plots of samples synthesized under the influence of TMEDA with their catalyst free counterparts with this information in mind, it becomes obvious that the large particle scattering signal is significantly broader in non-catalyzed samples. It can be therefore concluded that nanoparticles with high metallic character do have a correlation length, but it can not be accurately calculated from SAXS due to broad lines (probably caused by high size variance) and overlapping peaks.

The reaction temperature does not seem to have a strong effect on sample composition or morphology. The correlation length determined for samples synthesized at higher temperatures seems to be slightly larger, but also subject to greater variation than for samples synthesized at room temperature. Maybe clusters at the nm scale are more likely to collide and agglomerate to a bigger, more irregular cluster at these elevated temperatures.

The correlation lengths of nanoparticles synthesized under the influence of ultra sonication are very similar to their respective counterparts from conventional room temperature synthesis. In contrast to that, Reischauer found morphological changes of samples exposed to sonication on the μm scale [5]. It appears that sonication allows agglomeration of the nanostructures to larger microstructures, but does not increase the size of the nanostructures themselves. Their elemental compositions are not notably different from the other materials.

Overall these experiments show that through choosing the proper reaction conditions and particularly through TMEDA addition, the properties of the synthesized nanoparticles can be fine tuned by the operator. One important avenue for further research in this area is the use of additional analytical methods to complete the existing data. In particular, SEM, FESEM and TEM should be used more extensively for the investigation of the morphology in order to determine which differences in nano- and microstructure are causing the varying metallic character of different nanoparticles uncovered by scattering experiments. The samples should also be screened for conductivity so promising candidates can be selected for further electrochemical experiments such as cyclic voltammetry, in order to determine cycle stability and capacity and ultimately their viability as electrode material

for batteries,as these investigations of the electronic properties were unfortunately beyond the scope of this work. Additionally, a powder XRD measurement should be performed to confirm Sn(0) presence as the cause of the observed X-ray scattering. Parallel to these continued investigations into the model *o*-tolyl@Sn compound, further research should be put into the influence of the substituent on the eventual nanoparticle, particularly in view of the seemingly narrower particle size distribution of 1-naphthyl@Sn materials. The effect of a change in metal center to germanium could also provide new insights.

5 Experimental

5.1 Inert Gas Techniques

Unless otherwise specified, all reactions were carried out using standard schlenk line technique under an inert argon atmosphere. The argon gas was predried using a system from Air Liquide. Solvents were dried and deoxygenated using a system from "Innovative Technology Inc.", except for cyclohexane which was dried using a molecular sieve and stored under argon. Deionized H_2O was used for all experiments and degassed (where specified) by letting N_2 bubble through it overnight. $SnCl_4$ and TMEDA were distilled and stored under nitrogen. All final products of dehydrogenative coupling were stored in a glovebox under nitrogen atmosphere.

5.2 Chemicals

Table 5.1: Used chemicals and their sources

Chemical	**Source**
$SnCl_4$	Alfa Aesar
Mg	Merck
2-bromotoluene	Acros
1-bromonaphthalene	Acros
LAH	Sigma-Aldrich

5.3 SAXS and WAXS

A sample stage capable of mounting multiple different samples at once (Anton Paar, Graz) was filled with the powder inside the glove box. It was sealed by covering both sides with an adhesive tape (Scotch® Magic™ Tape) and carried to the analytical system inside an argon filled bucket to avoid air contamination. The measurements were carried out at room temperature in transmission mode on a SAXS-Point 2.0 (Anton Paar, Graz). Radiation was generated by a micro-X-ray source (Primux 100, Anton Paar,

Graz) producing Cu-K_α radiation (154.2 nm) at 50 W. Detection was performed by a 2D X-ray detector (EIGER R 1M, Dectris, Switzerland). SAXS was recorded at 542 mm sample-detector distance, WAXS at 77 mm.

5.4 Elemental Analysis

All samples for elemental analysis were prepared inside an argon filled glove box to ensure inert atmosphere. The measurements were carried out with an Elementar Vario EL III.

5.5 NMR

All NMR spectra were recorded at room temperature (22 °C) on a Mercury 300 MHz spectrometer from Varian. They were recorded at 300.22 MHz for ^{1}H, 75.5 MHz for ^{13}C and 111.92 MHz for ^{119}Sn. Unless otherwise specified, C_6D_6 was used as a solvent. The results are reported as chemical shifts relative to that of TMS (defined as 0) in parts per million (ppm). Singlets, duplets, triplets, quadruplets and multiplets are abbreviated as s, d, t, q and m respectively.

5.6 Microwave

Microwave experiments were performed in a Microwave Synthesis Reactor Monowave 300 (Anton Paar).

5.7 Supersonication

Supersonication experiments were performed on a Emmi 40H cleanig bath from EMAG. A seperate cryostat connected to a cooling coil was used for temperature regulation.

5.8 Scanning Electron Microscopy

The samples for SEM were fixated onto carbon tape on a sample holder inside the glove box. A vial was used to carry the sample holder to the analysis room while maintaining an inert atmosphere, where it was mounted onto a sputterer flushed with argon and covered in gold to ensure conductivity. The sample was then measured on a Vega 3 SBU SEM with a tungsten hair-pin cathode. Additionally, it was screened for oxidative damage with an INCA X-act EDX from Oxford Instruments.

5.9 Synthesis

5.9.1 List of compounds

Table 5.2: List of all synthesized compounds and materials

Class	Compound	Number
$aryl_4Sn$	*o*-$tolyl_4Sn$	**1**
	1-$naphthyl_4Sn$	**2**
$arylSnCl_3$	*o*-$tolylSnCl_3$	**3**
	1-$naphthylSnCl_3$	**4**
$arylSnH_3$	*o*-$tolylSnH_3$	**5**
	1-$naphthylSnH_3$	**6**
	o-tolyl@^{toluene}Sn	**7**
	o-tolyl@^{DME}Sn	**8**
	o-tolyl@^{benzene}Sn	**9**
	o-tolyl@^{cyclohexane}Sn	**10**
	o-tolyl@$^{toluene,\ TMEDA}$Sn	**11**
	o-tolyl@$^{DME,\ TMEDA}$Sn	**12**
	o-tolyl@$^{benzene,\ TMEDA}$Sn	**13**
	o-tolyl@$^{cyclohexane,\ TMEDA}$Sn	**14**
	o-tolyl@$^{toluene,\ 50\ °C}$Sn	**15**
	o-tolyl@$^{DME,\ 50\ °C}$Sn	**16**
	o-tolyl@$^{benzene,\ 50\ °C}$Sn	**17**
	o-tolyl@$^{cyclohexane,\ 50\ °C}$Sn	**18**
	o-tolyl@$^{toluene,\ TMEDA,\ 50\ °C}$Sn	**19**
	o-tolyl@$^{DME,\ TMEDA,\ 50\ °C}$Sn	**20**
	o-tolyl@$^{benzene,\ TMEDA,\ 50\ °C}$Sn	**21**
	o-tolyl@$^{cyclohexane,\ TMEDA,\ 50\ °C}$Sn	**22**
	o-tolyl@$^{toluene,\ TMEDA,\ son.}$Sn	**23**
	o-tolyl@$^{DME,\ TMEDA,\ son.}$Sn	**24**
	o-tolyl@$^{benzene,\ TMEDA,\ son.}$Sn	**25**
	o-tolyl@$^{cyclohexane,\ TMEDA,\ son.}$Sn	**26**
	1-naphthyl@$^{toluene,\ TMEDA}$Sn	**27**
	1-naphthyl@$^{DME,\ TMEDA}$Sn	**28**
	1-naphthyl@$^{benzene,\ TMEDA}$Sn	**29**
	1-naphthyl@$^{cyclohexane,\ TMEDA}$Sn	**30**

5.9.2 $ArSnH_3$

The steps towards the educt $ArSnH_3$ involve known compounds and have been adapted from known procedures [4, 15].

5.9.2.1 Ar_4Sn

A three neck flask equipped with a dropping funnel and a reflux condenser was charged with magnesium turnings (7 eq) in THF. The dropping funnel was charged with arylbromide (6 eq) in THF. 10 % of the arylbromide solution were added to the Mg suspension and the mixture was heated with a heatgun to start the reaction. Once clouding was visible, the heating was stopped and the rest of the arylbromide solution dripped in steadily over the course of 30 min. After the addition was complete, a heating mantle was put underneath the flask and the mixture stirred under reflux for 3 h. During this time, another flask containing THF was cooled in an ice bath. To this second flask, $SnCl_4$ (1 eq) was added under stirring. After 3 h, the Grignard reagent was poured onto the $SnCl_4$ through a bend containing packed glass wool. The mixture was stirred overnight, then refluxed with a heating mantle for another 2 h. Next, the solvent was removed under reduced pressure, resulting in a white solid. H_2O and CH_2Cl_2 were added, the setup was opened to ambient atmosphere and the mixture filtered through celite. The phases were separated and the aquatic phase extracted twice with CH_2Cl_2. The combined organic phases were dried over Na_2SO_4, filtered and the solvent removed at the rotavapor, affording a green oil. Et_2O was added to resuspend the desired product, resulting in fine, colorless crystals, which were filtered off, washed with Et_2O and dried under reduced pressure.

***o*-tolyl$_4$Sn (1):** Mg (8.00 g, 329 mmol) in THF (80 ml), 2-bromotoluene (34 ml, 48 g, 283 mmol) in THF (270 ml), $SnCl_4$ (5.5 ml, 12 g, 47 mmol) in THF (150 ml). Worked up with H_2O (200 ml) and CH_2Cl_2 (200 ml). Extracted with CH_2Cl_2 (2x200 ml). Resuspended in Et_2O (50 ml), then washed with Et_2O (2x20 ml).
Yield: 17 g (74 %)
^{1}HNMR (C_6D_6, 300 MHz): δ = 7.71 (d, 4H, ^3J(H6-H5) = 7.0 Hz, ^3J(H6-^{117}Sn) = 23 Hz, ^3J(H6-^{119}Sn = 30 Hz, H6), 7.20 - 7.12 (m, 4H, H4), 7.10 - 7.00 (m, 8H, H5 & H3), 2.28 (s, 12H, CH_3) ppm. ^{119}SnNMR (C_6D_6, 112 MHz): δ = -122.0 ppm.

1-naphthyl$_4$Sn (2): Mg (3.99 g, 164 mmol) in THF (50 mL), 1-bromonaphthalene (20 ml, 29.6 g, 143 mmol) in THF (280 ml), $SnCl_4$ (2.75 ml, 6.13 g, 23.5 mmol) in THF (200 ml). Worked up with H_2O and CH_2Cl_2. Extracted with CH_2Cl_2 (2x200 ml). Resuspended in Et_2O (50 ml), then washed with Et_2O (2x20 ml). Additionally washed with *n*–pentane (2x30 ml) to get rid of naphthalene.
Yield: 8.8 g (60 %)
^{1}HNMR (C_6D_6, 300 MHz): δ = 8.33 (d, 4H, ^3J(H4-H3) = 8.3 Hz), H4), 8.12 (d, 4H,

^3J(H2-H3) = 6.7 Hz, ^3J(H2-^{117}Sn) = 27.2 MHz, ^3J(H2-^{119}Sn) = 33.5 MHz, H2), 7.63 (d, 4H, ^3J(H8-H7) = 8.1 Hz, H8), 7.55 (d, 4H, ^3J(H5-H6) = 8.2), H5), 7.12 - 6.99 (m, 8H, H6 & H7), 6.83 (dd, 4H, ^3J(H3-H2,H4) = 7.6 Hz, H3) ppm. ^{119}SnNMR (C_6D_6, 112 MHz): δ = -118.8 ppm.

5.9.2.2 $ArSnCl_3$

A flask equipped with a reflux condenser was charged with Ar_4Sn (1 eq) and $SnCl_4$ (3.05 eq). It was heated to 150 °C, liquefying the Ar_4Sn in the process, then stirred for 2 hours. The excess of $SnCl_4$ was then removed under reduced pressure.

***o*-tolylSnCl$_3$ (3): 1** (16.9 g, 35 mmol) and $SnCl_4$ (12.8 ml, 28.5 g, 110 mmol). The liquid, red brown reaction product was filtered.
Yield: 40.4 g (88 %)
^{1}HNMR (C_6D_6, 300 MHz): δ = 7.22 (d, 1H, ^3J(H6-H5) = 7.5 Hz, ^3J(H6-^{117}Sn) = 61.5 Hz, ^3J(H6-^{119}Sn) = 68.5 Hz, H6), 7.00 (dd, 1H,^3J (H4-H5 & H4-H3) = 7.7 Hz, H4), 6.84 (dd, 1H,^3J (H5-H6 & H5-H4) = 7.4 Hz, H5), 6.78 (d, 1H,^3J (H3-H4) = 7.6 Hz, ^4J(H3-^{117}Sn) = 30.3 Hz, ^4J(H3-^{119}Sn) = 37.8 Hz, H3), 2.18 (s, 3H, CH_3) ppm. ^{119}SnNMR (C_6D_6, 112 MHz): δ = -63.8 ppm.

1-naphthylSnCl$_3$ (4): 2 (8.8g, 14.0 mmol) and $SnCl_4$ (5 ml, 11.2 g, 43 mmol). The solid reaction product was dissolved in CH_2Cl_2 (50 ml), filtered over celite and the solvent removed at the rotavapor. It was then recrystallized from toluene (15 ml) to afford colorless crystals which were dried under reduced pressure.
Yield: 8.3 g (42 %)
^{1}HNMR (C_6D_6, 300 MHz): δ = 7.95 - 9.90 (m, 1H, H8), 7.43 - 7.34 (m, 3H, H2 & H4 & H5), 7.09 - 7.04 (m, 2H, H6 & H7) 6.85 (dd, 1H, H3) ppm. ^{119}SnNMR (C_6D_6, 112 MHz): δ = -55.2 ppm.

5.9.2.3 $ArSnH_3$

A flask containing LAH (2 eq) in Et_2O was equipped with a dropping funnel, charged with $ArSnCl_3$ (1 eq) in Et_2O. It was cooled to -30 °C using an EtOH/N_2(l) mixture. The $ArSnCl_3$ was dripped in over 30 min under stirring. The cooling bath was switched for an ice bath and the mixture stirred another ten minutes. After that, excess LAH was quenched with degassed H_2O. The organic phase was cannuled onto $CaCl_2$, the aquatic phase extracted twice with Et_2O. The combined organic phases were removed from the drying agent with another cannula and the solvent removed under reduced pressure,

resulting in a dark orange liquid. It was purified through recondensation under vacuum produced by a turbomolecular pump from Ilmvac to afford the product as a colorless liquid.

***o*-tolylSnH$_3$**: LAH (2.40 g, 60.1 mmol) in Et_2O (50 ml), **3** (10.5 g, 31.5 mmol) in Et_2O (50 ml). Recondensed at room temperature.
Yield: 4.4 g (66 %)
^{1}HNMR (C_6D_6, 300 MHz): δ = 7.37 (d, 1H, ^3J(H6-H5) = 7.3 Hz, ^3J(H6-^{117}Sn) = 27.8 Hz, ^3J(H6-^{119}Sn) = 35.4 Hz, H6), 7.10 (dd, 1H, ^3J(H5-H6 & H5-H4) = 7.1 Hz), H5, 7.02 - 6.92 (m, 2H, H2 & H3), ^1J(H-^{117}Sn) = 913 Hz, ^1J(H-^{119}Sn) = 955 Hz, 4,96 (s, 1H, SnH_3), 2.15 (s, 1H, CH_3) ppm. ^{119}SnNMR (C_6D_6, 112 MHz): δ = -361 (q, ^1J(^{119}Sn-^{1}H) = 1907 Hz) ppm.

1-naphthylSnCl$_3$ (4):: LAH (3.5 g, 92 mmol) in Et_2O (50 ml) and **2** (16 g, 45 mmol) in Et_2O (50 ml). Recondensed at 50 °C using a water bath.
Yield: 3.4 g (30 %)
^{1}HNMR (C_6D_6, 300 MHz): δ = 7.70 - 7.63 (m, 1H, H8), 7.59 - 7.53 (m, 2H, H4 & H5), 7.48 (d, 1H, ^3J(H2-H3) = 6.6 Hz, H2), 7.24 - 7.18 (m, 2H, H6 & H7), 7.11 (dd, 1H, ^3J(H3-H4 & H3-H2) = 7.3 Hz, H3), 5.12 (s, 3H, SnH_3) ppm. ^{119}SnNMR (C_6D_6, 112 MHz): δ = 355 (q, ^1J(^{119}Sn-^{1}H) = 1950 Hz) ppm.

5.9.3 Coupling at Room Temperature

$ArSnH_3$ (0.3 ml) was dissolved in solvent (5 ml) in a 50 ml schlenk flask equipped with a stir bar. For base catalyzed reactions, TMEDA (0.3 ml, 233 ml, 2.0 mmol) was added. The flask was then closed and stirred until black solid had formed and the supernatant was clear. Catalyzed reactions stayed connected to the schlenk line for the entire reaction duration (ca. 30 min) to ensure pressure equalization, uncatalyzed reactions were equalized once per week.
7: **5** in toluene
8: **5** in DME
9: **5** in benzene
10: **5** in cyclohexane
11: **5** with TMEDA in toluene
12: **5** with TMEDA in DME
13: **5** with TMEDA in benzene
14: **5** with TMEDA in cyclohexane
27: **6** with TMEDA in toluene

28: **6** with TMEDA in DME
29: **6** with TMEDA in benzene
30: **6** with TMEDA in cyclohexane

5.9.4 Coupling Induced by Conventional Heat

Solvent (5 ml) was prepared in a schlenk flask equipped with a stir bar. For catalyzed reactions, TMEDA (0.3 ml, 233 ml, 2.0 mmol) was added. The solution was heated to 50 °C (±5 °C) and $ArSnH_3$ added, then it was stirred until black solid had formed and the supernatant was clear. Catalyzed reactions stayed connected to the schlenk line for the entire reaction duration, uncatalyzed reactions were pressure equalized once per day.
15: **5** in toluene
16: **5** in DME
17: **5** in benzene
18: **5** in cyclohexane
19: **5** with TMEDA in toluene
20: **5** with TMEDA in DME
21: **5** with TMEDA in benzene
22: **5** with TMEDA in cyclohexane

5.9.5 Coupling induced by supersonication

A schlenk flask was charged with $ArSnH_3$ (0.3 ml) and solvent (5 ml). The flask was put into a sonication bath. For catalyzed reactions, TMEDA was then added. The flask was sonicated until black solid had formed and the supernatant was clear.
23: **5** with TMEDA in toluene
24: **5** with TMEDA in DME
25: **5** with TMEDA in benzene
26: **5** with TMEDA in cyclohexane

5.10 Workup of Nanoparticles

A centrifuge (Rotanta 460 from Hettich) was used to separate the nanoparticles and see whether the supernatant is clear. The solvent was then removed under reduced pressure. For materials containing a 1-naphthyl substituent, the solvent was then kept at reduced

pressure (about 0.1 mbar) for one hour while simultaneously being warmed to 50 °C in a water bath to remove naphthalene. Then the nanoparticles were moved from the flask into a vial inside the glove box for long term storage.

6 Abbreviations

Me - methyl
Et - ethyl
Pr - propyl
Bu - butyl
Oct - octyl
Ph - phenyl
t - *tert*
o - *ortho*
DCM - dichloromethane
DME - 1,2-dimethoyethane
Et_2O - diethyl ether
LAH - lithium aluminum hydride ($LiAlH_4$)
THF - tetrahydrofuran
TMEDA - N,N,N',N'-tetramethylethane-1,2-diamine
TMS - tetramethylsilane
EA - elemental analysis
EDX - energy dispersive X-ray analysis FESEM - field emission scanning electron microscope
GC/MS - gas chromatography-mass spectrometry
GPC - gel permeation chromatography
NMR - nuclear magnetic resonance
SAXS - small-angle X-ray scattering
SEM - scanning electron microscope
TEM - transmission electron microscope
WAXS- wide-angel X-ray scattering
XRD - X-ray diffraction
RT - room temperature

7 References

(1) Zuo, X.; Zhu, J.; Müller-Buschbaum, P.; Cheng, Y.-J. *Nano Energy* **2017**, *31*, 113–143.

(2) Wang, B.; Luo, B.; Li, X.; Zhi, L. *Materials Today* **2012**, *15*, 544–552.

(3) XIE, H.-m.; VAN, X.-d.; YU, H.-y.; ZHANG, L.-y.; YANG, G.-l.; XU, Y.; WANG, R.-s. *Chemical Research in Chinese Universities* **2006**, *22*, 639–642.

(4) Zeppek, C. Amine Base Induced Polymerization of Aryltin Hydrides: Mechanistic Insights & Nanomaterial Characterization, Doctoral Thesis, Graz University of Technology, 2015.

(5) Reischauer, S. Polymerization of Tin Hydrides: Influence of Methods on Material Formation, MASTER'S THESIS, Graz University of Technology, 2018.

(6) Paneth, F.; Fürth, K. *Berichte der deutschen chemischen Gesellschaft (A and B Series)* **1919**, *52*, 2020–2029.

(7) Paneth, F.; Rabinowitsch, E. *Berichte der deutschen chemischen Gesellschaft (A and B Series)* **1924**, *57*, 1877–1890.

(8) Kraus, C. A.; Greer, W. N. *Journal of the American Chemical Society* **1922**, *44*, 2629–2633.

(9) Chambers, R. F.; Scherer, P. C. *Journal of the American Chemical Society* **1926**, *48*, 1054–1062.

(10) Finholt, A. E.; Bond, A. C.; Wilzbach, K. E.; Schlesinger, H. I. *Journal of the American Chemical Society* **1947**, *69*, 2692–2696.

(11) Sasin, R.; Sasin, G. S. *The Journal of Organic Chemistry* **1955**, *20*, 770–773.

(12) Dillard, C. R.; McNeill, E. H.; Simmons, D. E.; Yeldell, J. B. *Journal of the American Chemical Society* **1958**, *80*, 3607–3609.

(13) Anderson, H. H. *Journal of the American Chemical Society* **1957**, *79*, 4913–4915.

(14) Ingham, R. K.; Rosenberg, S. D.; Gilman, H. *Chemical Reviews* **1960**, *60*, 459–539.

(15) Zeppek, C.; Pichler, J.; Torvisco, A.; Flock, M.; Uhlig, F. *Journal of Organometallic Chemistry* **2013**, *740*, 41–49.

(16) Zeppek, C.; Fischer, R. C.; Torvisco, A.; Uhlig, F. *Canadian Journal of Chemistry* **2014**, *92*, 556–564.

(17) Schittelkopf, K.; Fischer, R. C.; Meyer, S.; Wilfling, P.; Uhlig, F. *Applied Organometallic Chemistry* **2010**, *24*, 897–901.

(18) Voronkov, M. G.; Abzaeva, K. A. In *The Chemistry of Organic Germanium, Tin and Lead Compounds*; John Wiley & Sons, Ltd: 2002, pp 1–130.

(19) Voronkov, M. G.; Egorochkin, A. N. In *The Chemistry of Organic Germanium, Tin and Lead Compounds*; John Wiley & Sons, Ltd: 2002, pp 131–168.

(20) Voronkov, M. G.; Adamovich, S. N.; Khramtsova, S. Y.; Shternberg, B. Z.; Rakhlin, V. I.; Mirskov, R. G. *Bulletin of the Academy of Sciences of the USSR Division of Chemical Science* **1987**, *36*, 1317–1319.

(21) Caseri, W. *Chemical Society Reviews* **2016**, *45*, 5187–5199.

(22) Löwig, C. *Journal für Praktische Chemie* **1852**, *57*, 385–434.

(23) Caseri, W. *Journal of Organometallic Chemistry* **2014**, *751*, 20–24.

(24) Strecker, A. *Annalen der Chemie und Pharmacie* **1858**, *105*, 299–320.

(25) Cahours, A. *Annalen der Chemie und Pharmacie* **1860**, *114*, 227–255.

(26) Frankland, E. *Philosophical Transactions of the Royal Society of London* **1852**, *142*, 417–444.

(27) Imori, T.; Lu, V.; Cai, H.; Tilley, T. D. *Journal of the American Chemical Society* **1995**, *117*, 9931–9940.

(28) Miles, D.; Burrow, T.; Lough, A.; Foucher, D. *Journal of Inorganic and Organometallic Polymers and Materials* **2010**, *20*, 544–553.

(29) Devylder, N.; Hill, M.; Molloy, K. C.; Price, G. J. *Chemical Communications* **1996**, 711.

(30) Trummer, M.; Solenthaler, D.; Smith, P.; Caseri, W. *RSC Advances* **2011**, *1*, 823.

(31) Trummer, M.; Choffat, F.; Rämi, M.; Smith, P.; Caseri, W. *Phosphorus, Sulfur, and Silicon and the Related Elements* **2011**, *186*, 1330–1332.

(32) Lechner, M.-L.; Trummer, M.; Bräunlich, I.; Smith, P.; Caseri, W.; Uhlig, F. *Applied Organometallic Chemistry* **2011**, *25*, 769–776.

(33) Holder, S. J.; Jones, R. G.; Benfield, R. E.; Went, M. J. *Polymer* **1996**, *37*, 3477–3479.

(34) Elangovan, M.; Muthukumaran, A.; Kulandainathan, M. A. *Materials Letters* **2006**, *60*, 1099–1105.

(35) Neumann, W. P.; König, K. *Angewandte Chemie International Edition in English* **1962**, *1*, 212–213.

(36) Neumann, W. P.; König, K. *Justus Liebigs Annalen der Chemie* **1964**, *677*, 1–11.

(37) Davies, A. G.; Osei-Kissi, D. K. *Journal of Organometallic Chemistry* **1994**, *474*, C8–C10.

(38) Sindlinger, C. P.; Wesemann, L. *Chemical Science* **2014**, *5*, 2739–2746.

(39) Sindlinger, C. P.; Stasch, A.; Bettinger, H. F.; Wesemann, L. *Chemical Science* **2015**, *6*, 4737–4751.

(40) Maudrich, J.-J.; Sindlinger, C. P.; Aicher, F. S. W.; Eichele, K.; Schubert, H.; Wesemann, L. *Chemistry - A European Journal* **2017**, *23*, 2192–2200.

(41) Neumann, W. P.; Schneider, B. *Angewandte Chemie* **1964**, *76*, 891–891.

(42) Sommer, R.; Neumann, W.; Schneider, B. *Tetrahedron Letters* **1964**, *5*, 3875–3878.

(43) Costisella, B.; Englich, U.; Prass, I.; Schürmann, M.; Ruhlandt-Senge, K.; Uhlig, F. *Organometallics* **2000**, *19*, 2546–2550.

(44) Harrypersad, S.; Liao, L.; Khan, A.; Wylie, R. S.; Foucher, D. A. *Journal of Inorganic and Organometallic Polymers and Materials* **2015**, *25*, 515–528.

(45) Harrypersad, S.; Foucher, D. *Chemical Communications* **2015**, *51*, 7120–7123.

(46) Dhindsa, J. S.; Jacobs, B. F.; Lough, A. J.; Foucher, D. A. *Dalton Transactions* **2018**, *47*, 14094–14100.

(47) Imori, T.; Tilley, T. D. *Journal of the Chemical Society, Chemical Communications* **1993**, 1607.

(48) Lu, V.; Tilley, T. D. *Macromolecules* **1996**, *29*, 5763–5764.

(49) Lu, V. Y.; Tilley, T. D. *Macromolecules* **2000**, *33*, 2403–2412.

(50) Babcock, J. R.; Sita, L. R. *Journal of the American Chemical Society* **1996**, *118*, 12481–12482.

(51) Thompson, S. M.; Schubert, U. *Inorganica Chimica Acta* **2003**, *350*, 329–338.

(52) Neale, N. R.; Tilley, T. D. *Journal of the American Chemical Society* **2002**, *124*, 3802–3803.

(53) Neale, N. R.; Tilley, T. *Tetrahedron* **2004**, *60*, 7247–7260.

(54) Choffat, F.; Buchmüller, Y.; Mensing, C.; Smith, P.; Caseri, W. *Journal of Inorganic and Organometallic Polymers and Materials* **2009**, *19*, 166–175.

(55) Sharma, H.; Arias-Ugarte, R.; Metta-Magana, A.; Pannell, K. *Angewandte Chemie* **2009**, *121*, 6427–6430.

(56) Choffat, F.; Smith, P.; Caseri, W. *Journal of Materials Chemistry* **2005**, *15*, 1789.

(57) Okano, M.; Matsumoto, N.; Arakawa, M.; Tsuruta, T.; Hamano, H. *Chemical Communications* **1998**, 1799–1800.

(58) Okano, M.; Watanabe, K.; Totsuka, S. *Electrochemistry* **2003**, *71*, 257–259.

(59) Darwish, A.; Chong, J. M. *Synthetic Communications* **2004**, *34*, 1885–1890.

(60) Khan, A.; Gossage, R. A.; Foucher, D. A. *Canadian Journal of Chemistry* **2010**, *88*, 1046–1052.

(61) Pau, J.; Lough, A. J.; Wylie, R. S.; Gossage, R. A.; Foucher, D. A. *Chemistry - A European Journal* **2017**, *23*, 14367–14374.

(62) Takeda, K.; Shiraishi, K. *Chemical Physics Letters* **1992**, *195*, 121–126.

(63) Adams, S.; Dräger, M. *Angewandte Chemie International Edition in English* **1987**, *26*, 1255–1256.

(64) Choffat, F.; Käser, S.; Wolfer, P.; Schmid, D.; Mezzenga, R.; Smith, P.; Caseri, W. *Macromolecules* **2007**, *40*, 7878–7889.

(65) Sekiguchi, A.; Sakurai, H. In *Advances in Organometallic Chemistry*; Elsevier: 1995, pp 1–38.

(66) Sita, L. R.; Bickerstaff, R. D. *Journal of the American Chemical Society* **1989**, *111*, 6454–6456.

(67) Wiberg, N.; Lemer, H.-W.; Wagner, S.; Nöth, H.; Seifert, T. *Zeitschrift für Naturforschung B* **1999**, *54*, 877–880.

(68) Eichler, B. E.; Power, P. P. *Angewandte Chemie* **2001**, *113*, 818–819.

(69) Richards, A. F.; Eichler, B. E.; Brynda, M.; Olmstead, M. M.; Power, P. P. *Angewandte Chemie International Edition* **2005**, *44*, 2546–2549.

(70) Schnepf, A. *Angewandte Chemie International Edition* **2004**, *43*, 664–666.

(71) Gómez, A. T.; Uhlig, F.; Scheschkewitz, D., *Smart Inorganic Polymers: Synthesis, Properties, and Emerging Applications in Materials and Life Sciences.* Hey-Hawkins, E., Hissler, M., Eds.; Wiley-VCH: Weinheim, Germany, 2019; Chapter Synthesis of Group 14 Metal-Containing Polymers, pp 61–84.

(72) Oehl, N.; Schmuelling, G.; Knipper, M.; Kloepsch, R.; Placke, T.; Kolny-Olesiak, J.; Plaggenborg, T.; Winter, M.; Parisi, J. *CrystEngComm* **2015**, *17*, 8500–8504.

(73) Reischauer, S. unpublished results, TU Graz, 2018.

8 List of Figures

9 List of Tables